POLITECNICO DI TORINO

DOCTORAL SCHOOL

Ph.D. in Production Systems & Industrial Design

Cycle XXVIII

Dissertation

Study and Characterization of a Camera-based Distributed System for Large-Volume Dimensional Metrology Applications

PhD Candidate: Ou BAI

Supervisor:
Prof. Maurizio Galetto

Chairman:
Prof. Luca Settineri

March 2016

Acknowledgements

This dissertation presents joint work with Professor Franceschini, Maurizio Galetto, Augusto Maisano and Luca Mastrogiacomo. I thank them all for their fruitful collaboration and the insightful advices, and I am deeply grateful for their help in the completion of this dissertation. Particularly I wish to thank my supervisor Professor Maurizio Galetto for his constant helpfulness and guidance on improving my research work.

Furthermore, I wish to thank Professor Mark Williams and Jafar Jamshidi from WMG (Warwick Manufacturing Group) of University of Warwick, UK, for their warm-hearted help and guidance in my visit to University of Warwick.

Besides, I sincerely extend my thanks to Professor Luca Settineri, Dr. Gianfranco Genta and Mr. Marchiandi Giovanni, for their kind help in my research career.

Finally, I want to thank my wonderful family for the invaluable support and encouragement.

Executive summary

Large-Volume Dimensional Metrology (LVDM) deals with dimensional inspection of large objects with dimensions in the order of tens up to hundreds of meters. Typical large volume dimensional metrology applications concern the assembly/disassembly phase of large objects, referring to industrial engineering. Based on different technologies and measurement principles, a wealth of LVDM systems have been proposed and developed in the literature, just to name a few, e.g., optical based systems such as laser tracker, laser radar, and mechanical based systems such as gantry CMM and multi-joints artificial arm CMM, and so on. Basically, the main existing LVDM systems can be divided into two categories, i.e. centralized systems and distributed systems, according to the scheme of hardware configuration. By definition, a centralized system is a stand-alone unit which works independently to provide measurements of a spatial point, while a distributed system, is defined as a system that consists of a series of sensors which work cooperatively to provide measurements of a spatial point, and usually individual sensor cannot measure the coordinates separately. Some representative distributed systems in the literature are iGPS, MScMS-II, and etc. The current trend of LVDM systems seem to orient towards distributed systems, and actually, distributed systems demonstrate many advantages that distinguish themselves from conventional centralized systems.

This dissertation originates from the research activity carried out at the Industrial Metrology and Quality Engineering Laboratory of DIGEP – Politecnico di Torino within the framework of a distributed system for Large-Volume Dimensional Metrology applications (Mobile Spatial coordinate Measuring System). Whereas two prototypes have been established – the MScMS-I (exploited with Ultra-Sound technology) and the MScMS-II (exploited with Infrared technology), the novelty of proposed solution (namely, custom-made multi-camera system), based on generic CCD sensors (sensible to visible light, as well as Infrared light), sharing similar hardware organization and working principles, outperforms the previous two systems in metrological performance, and presents several advantages as well. Besides, a new concept of probe involved in the system for defining the point to be measured is proposed in the dissertation, which is designed to be an active, smart and modular probe, and the new probe enhances the functions of a generic probe with the capabilities of monitoring the environmental factors, and refining the measurement results of a spatial point by compensating and correcting those external influences.

This dissertation contains a detailed description of the working principles and the implementation of MScMS-II. Then, the error correction method and calibration strategy of the system are presented and discussed. Afterwards, the implementation of hardware scheme and development of associated software with the proposed system are presented, followed by a comparison between the new system and MScMS-II.

Content

List of acronyms and abbreviations

2D	two-dimensional
3D	three-dimensional
ADM	Absolute Distance Meter
CAD	Computer Aided Design
CCD	Charge-Coupled Device
CLR	Coherent Laser Radar
CMM	Coordinate Measuring Machine
DIGEP	Dipartimento di Ingegneria Gestionale E della Produzione
DOF	Degrees Of Freedom
DPU	Data Processing Unit
FMCW	Frequency-Moduled Continuous-Wave
FOV	Field Of View
GUI	Graphical User Interface
iGPS	Indoor Global Positioning System
IFM	Interferometer
IR	InfraRed
LED	Light Emitting Diode
LSDM	Large-Scale Dimensional Metrology
MOT	Multi-Object Tracking
MScMS	Mobile Spatial coordinate Measuring System
NURBS	Non-Uniform Rational B-Spline
PC	Personal Computer
RANSAC	RANdom SAmple Consensus
SMR	Spherically Mounted Retro-reflector
WCS	World Coordinate System

1. Introduction and Literature Review

Large-Scale/Large-Volume Dimensional Metrology (LSDM) is that branch of metrology dealing with "objects with linear dimensions ranging from tens to hundreds of meters" (M. J. Puttock 1978). Last decades has shown a great deal of applications of LSDM, involving different arenas of technology, ranging from civil and industrial architecture to aerospace engineering. Referring to industrial engineering, the most typical applications of LSDM systems concern the assembly/disassembly phase and/or in-situ dimensional tolerancing of large-volume objects (F. Franceschini et al. 2014). Many examples reported in scientific literature confirm this tendency (P. G. Maropoulos et al. 2008, J. Jamshidi et al. 2010). Other typical applications are for reverse engineering and tracking of automated arms or moving robots (A. Nüchter et al. 2003, E. Savio et al. 2007, M. Galetto et al. 2010c, J. Santolaria et al. 2013).

1.1 Introduction to main existing LSDM systems

Based on different technologies (optical, mechanical, electromagnetic etc.) and measuring principles (angle, distance, or hybrid measurement), a wealth of LSDM systems have been proposed in the literature and developed according to different design requirements, just to name a few, such as laser trackers (firstly proposed in 1980s, by Lau and Hocken (Kam C Lau and Robert J Hocken 1987)) and laser radar (FARO , Nikon Metrology NV), traditional CMMs (e.g. gantry and horizontal-arm CMMs) (Hexagon , Konica Minolta , Nikon Metrology NV , D. A. Maisano et al. 2009), iGPS^{TM} and distributed systems (J. E. Muelaner et al. 2010, R. Schmitt et al. 2010, F. Du et al. 2012, A. R. Norman et al. 2013), and photogrammetric systems (A. W. Burner et al. 1997, M. Ribo and M. Brandner 2005, Thomas Luhmann et al. 2006, J. Fryer et al. 2007, Maurizio Galetto et al. 2010a, M. Galetto et al. 2010b, M. Galetto et al. 2010a). A rough scheme about the temporal evolution of the main families of LSDM systems and relating accuracy is reported in Fig. 1-1, and a detailed introduction about some state-of-the-art systems is as follows:

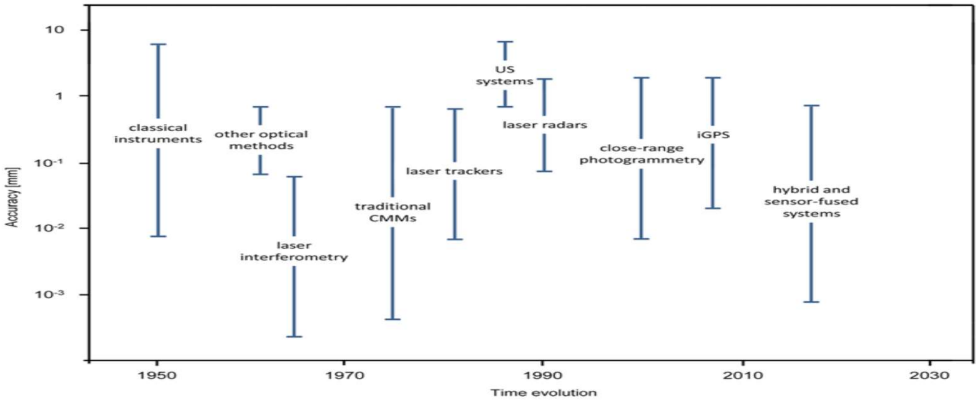

Fig. 1-1 Evolution of the main families of LSDM systems and relating accuracy over time (F. Franceschini et al. 2014). (with permission)

- Laser tracker: since its first introduction by Lau and Hocken in 1980s, laser tracker is still extensively used for large-scale industrial and scientific metrology. Current laser trackers, based on the combined use of built-in Absolute Distance Meter (ADM) and Relative-Displacement-Measuring Interferometer (IFM), have overcome the drawback that only permitted the measurement of a displacement from a datum position since just IFM was equipped. This makes more practical and easier the use of laser trackers because the ADM permits the resetting of the measuring system without having to return the retro-reflector to the datum position. The introduction of the most recent versions of laser trackers, only based on ADM technology, has improved significantly the acquisition speed, giving almost real-time distance measurement performance, even though assuring high levels of accuracy (typically 10±0.4 μm/m) (FARO , Hexagon , Konica Minolta , API Automated Precision). A further improvement of laser trackers has been obtained in the last years with the introduction of specific 6DOF probes able to return the exact position of the touched point or (depending on the characteristics of the specific probe) a local scansion of the portion of the measured surface (FARO , API Automated Precision).
- Traditional CMMs: traditional gantry and horizontal-arm CMMs are still largely employed systems for LSDM applications (Hexagon , Konica Minolta , Nikon Metrology NV , F. Franceschini et al. 2009). A typical CMM is composed of three axes, X, Y and Z. These axes are orthogonal to each other in a typical three-dimensional coordinate system. Each axis has a scale system that indicates the location of that axis. Measurements are defined by a probe attached to the third moving axis of this machine. The machine reads the input from the touch probe, as directed by the operator or programmer. The machine then uses the X, Y, Z coordinates of each of these points to determine size and position with micrometer precision typically. Probes may be mechanical, optical (Simone Carmignato 2009), laser, or white light, amongst others (Wikipedia). Nevertheless, even if they assure a very high level of accuracy (from 10μm+L/200 (Nikon Metrology NV)) and advantage of providing the coordinate measurement of (potentially) all sides of the measured object, their use is strongly limited by two restrictions, which often represent inevitable exclusion elements for their employment in many operative contexts:
  (i) the first one is the impossibility of moving the CMM to the measurement object, hence no in-situ measurement can be performed and the measured object must always be transported to the CMM laboratory;
  (ii) the second one is related to its monolithic structure in which the probe is always joined to the main frame through a specific arm, this prevents the free movement of the probe inside the measurement volume without colliding with the measured object.
- Laser radars: Coherent Laser Radars (CLR) are the immediate alternative to laser trackers, they allow fast and accurate measurement of surfaces without needing collaborative markers (FARO , Nikon Metrology NV). CLR technology is based on the principle of Frequency-Moduled Continuous-Wave (FMCW), which permits to obtain absolute distance measurements without the use of specific cooperative markers, analyzing the

coherent interference of an opportunely shaped Infrared (IR) signal and the corresponding reflected signal from the target surface (Tony Slotwinski and Patrick Blanckaert 2007). Although this technology does not ensure the same level of accuracy of laser trackers, it presents remarkable advantages in terms of data density, even over large surfaces, and the ability to measure non-cooperative markers and featureless surfaces.

- iGPS and distributed systems: One of the most interesting systems recently introduced in the field of LSDM is the Indoor-GPS (iGPS), which is a successful example of a category of instruments identified as Rotary-Laser Automatic Theodolites (R-LAT) (J. E. Muelaner et al. 2010, R. Schmitt et al. 2010, F. Du et al. 2012, A. R. Norman et al. 2013). The system components of iGPS are a network of transmitters, a control center and a number of wireless probe sensors. Transmitters use laser and infrared light to determine the relative angles from the transmitters to the probe-sensors. These latters have photodiodes inside their modules that can sense the transmitted laser and infrared light signals. Based on the known location of the transmitters, which is normally obtained in an initial network calibration phase, the position of the sensors can be subsequently calculated (Nikon Metrology NV , Jody E Muelaner et al. 2008). In short, from the operational point of view, iGPS shares similarities with traditional theodolite surveying and GPS (Global Positioning System) navigation systems.
- Digital photogrammetry: the fundamental principle used by photogrammetry is triangulation. By taking photographs or video images from at least two different locations, so-called "lines of sight" can be developed from each camera to points on the object. These lines of sight (sometimes called rays owning to their optical nature) are mathematically intersected to produce the 3-dimensional coordinates of the points of interest (A. W. Burner et al. 1997, M. Ribo and M. Brandner 2005, Thomas Luhmann et al. 2006, J. Fryer et al. 2007, Maurizio Galetto et al. 2010a, M. Galetto et al. 2010b, M. Galetto et al. 2010a). It is easy to understand that when photogrammetry was based on traditional photograph, the elaboration was difficult and required quite a bit of time. With the introduction of digital cameras, and the consequent transformation in digital photogrammetry, measurement time reduced enormously, allowing real time tracking, and the level of accuracy became comparable to other LSDM systems. The great advantage of digital photogrammetry is to provide a non-contact method for determining surface shape, position and orientation that is particularly suited to the monitoring of movement and change over time (Thomas Luhmann et al. 2006, F. Franceschini et al. 2014).
- Hybrid systems: a separate subject concerns the so called "hybrid systems", that is all systems obtained by integrating two or more different technologies (G. N. Peggs et al. 2009). Typical examples of this kind of systems are total stations, essentially composed by theodolites with added distance measurement capability (B Aebischer and B Braunecker 2003). The advantage of hybrid systems is that they can incorporate all the advantages of different instruments they integrate. Typical integration refers to laser scanning and close-range photogrammetry or structured light, furthermore, great

advantages can be reached by equipping automatic systems with video image devices (F. Franceschini et al. 2014). Considering all the possible combinations, a multitude of different types of hybrid optical-based measuring systems can be imagined, with their advantages and drawbacks. An interesting review of traditional and less known optical techniques is provided by (F. Chen et al. 2000).

- Other metrological systems: to name a few, such as laser line scanners, structured light and shading methods systems, ultrasound systems (e.g. MScMS-I) etc. The study of these systems is beyond the goal of this thesis, for detailed introduction, please refer to the references (Paul Debrule et al. 1995, Joaquim Salvi et al. 2004, M. Ribo and M. Brandner 2005, Song Zhang and Peisen S Huang 2006, D. A. Maisano et al. 2009, Nick Van Gestel et al. 2009).

1.2 Classification of LSDM systems

A comprehensive taxonomy was proposed to analysis and classify the main existing LSDM systems, based on five perspectives detailed with several criteria in each perspective (F. Franceschini et al. 2014), according to the goal of study of this thesis, only 3 criteria are focused: (i) hardware organization (centralized or distributed systems); (ii) interaction with the measured object (contact or non-contact systems); and (iii) measurement principle (angle and/or length measurement approaches). A detailed definition and explanation of the taxonomy is outlined as follows.

- Centralized system: a centralized system is essentially a stand-alone unit which can work independently to provide the measurement of a spatial coordinate on the object surface, e.g. a laser tracker. In some cases, a number of centralized systems can be used simultaneously with the aim of improving measurement accuracy.
- Distributed system: a distributed system consists in a series of sensors that work cooperatively to collect information for determining coordinates of a point on the object's geometry. In general, the individual sensors associated with a distributed system cannot measure coordinates separately (e.g. iGPS, ultrasound systems and distributed camera systems).
- Contact system: a contact measuring system is a metrological system which can provide the coordinate of the object to be measured simply by touching it with a probe (e.g. wireless probe sensors of iGPS system) or a target (e.g. SMR (spherically mounted retroreflector) of laser tracker). The probe or the target of the metrological system can be moved either manually or by mechanical arms or can be attached to the object as a target to be followed by the system.
- Non-contact system: a non-contact system can evaluate dimensional features of the object to be measured without the need for a probe (or target) to touch the object. They are mainly based on optical technologies (e.g. laser radar, optical-probe CMM, photogrammetry system).

- Multiple angles method: the method based on multiple angles relies on the well-known triangulation principle. The position of a point in three-dimensional space is evaluated according to the know locations and/or attitudes of two or more reference points (or sensors) and relative measured angles between the point to be localized and each reference point (or sensor) (Kutluyil Doğançay 2005). Camera-based triangulation, iGPS, photogrammetry are examples that adopt multiple angles method.
- Multiple lengths method: the method based multiple lengths, which implement trilateration principles, uses the known spatial location of three of more reference points (or sensors) and the measured distance between the point to be localized and each reference point (or sensor) (Bernhard Hofmann-Wellenhof et al. 2012), CMMs, multiple laser trackers are examples based on this method.
- Two angles and one length method: this method locates a point with reference to a spherical coordinate system, by measuring angles through angular encoders and length through interferometers and/or ADM. Laser tracker, laser radar and total stations are examples classified in this method.

A summary of main existing LSDM solutions classified respecting to the above mentioned criteria is shown in table 1-1:

Table 1-1 Classification of major LSDM systems.

Interaction with measured object	**Measurement Principle**	**Hardware organization** *Centralized*	*Distributed*
Contact	*Multiple angles*	Single/stereo camera based systems	iGPS, multi camera based systems
	Multiple lengths	CMMs	Ultrasound systems, multilateral use of laser trackers
	Two angles and one length	Laser trackers, total stations	
Non-contact	*Multiple angles*	Digital photogrammetry systems	Multi camera based systems
	Multiple lengths	Tacheometers	
	Two angles and one length	Theodolites, laser radars	

The current trend of LSDM systems seems oriented towards distributed systems, i.e., systems composed by different typology of devices, (all together) cooperating in order to pursue the common objective of giving a measurement result as much as accurate and precise as possible, reliable, repeatable and stable over time (F. Franceschini et al. 2014). This is the case, for example, of laser tracker multilateration systems and laser trackers and photogrammetry integrated systems (Toshiyuki Takatsuji et al. 1998, EB Hughes et al. 2000, J. Mitchell et al. 2004, K Wendt et al. 2010, H. González-Jorge et al. 2012).

1.3 Generic architecture and state-of-the-art analysis of LSDM system

Distributed metrological systems have a common architecture, consisting of (i) a network of spatially distributed sensors, within the working volume; (ii) a portable probe to touch the point to be measured; and (iii) a centralized data processing unit (DPU) to acquire and process measurement data and to elaborate them according to the measurement task. Actually they demonstrate many advantages that distinguish them from conventional centralized systems (Fiorenzo Franceschini et al. 2011), such as:

- *Flexibility:* distributed systems can easily allocate multiple sensors in the working volume according to user requirements, the geometry of the environment, and the measurement tasks. By implementing pre-processing software to find possible optimal configuration layouts, the flexibility can be furtherly enhanced, as well as the metrological performance and/or the measurement volume (M. Galetto, Pralio B 2010).
- *Reliability:* reliability is the ability of a system to perform and maintain its functions in routine circumstances, as well as in hostile or unexpected circumstances (Fiorenzo Franceschini et al. 2011). If some of the distributed sensors are not in good function, the whole metrology system, characterized by hardware redundancy, can still use remaining sensors to compensate for the malfunctioning of a portion of the sensors.
- *Scalability:* a great advantage of a distributed system is the capability to cover a large working volume and unusual shapes. The actual working volume of a distributed metrology system is related to its sensors' layout. The density and/or position of the sensors can be easily adapted to the user's requirements, within the network design phase and/or during the experiments.
- *Concurrent measurement capability:* distributed metrology systems generally allow concurrent use of different measurement tools (e.g. targets, portable probes, etc.). Once the sensor network has been set up, theoretically an unlimited number of tools can be integrated within the working volume, without additional cost per user.
- *Sensor fusion:* Other spatially distributed sensors (e.g. thermometer, hygrometer, gyroscope, light-sensitive unit, etc.) can be integrated to the metrology system, in order to monitor temperature, humidity, vibrations, environmental light intensity, etc. Sensor fusion makes it possible to define a composite mapping of the metrological performance against the operating conditions.

1.4 Main goal and organization of this thesis

The main goal of this thesis is to study and characterize an optical-based LSDM solution, i.e. the IR-based innovative indoor coordinate measuring system (MScMS-II, by (Maurizio Galetto et al. 2010a)), and to discuss the possible improvement within the MScMS-II framework, in large-volume metrology applications. The remainder of this dissertation contains a detailed description of the working principles and the implementation of MScMS-II. Then, the error correction method and calibration strategy of the system are presented and discussed. More specifically, the thesis is structured like this:

- Chap. 2 presents a comprehensive description of the MScMS-II system and proposes a conceptual design of smart probe involved in the system;
- Chap. 3 introduces a series of error correction methods adapted to the MScMS-II system;
- Chap. 4 concentrates the development a diagnostic technique based on multivariate control charts for monitoring the system stability;
- Chap. 5 presents the development of a generic CCD camera-based distributed system within MScMS-II framework;
- Chap. 6 concludes the research with main results achieved and summarizes the original contributions of the thesis.

2. Study of an IR-based LSDM system: MScMS-II

2.1 Introduction

The purpose of this chapter is to present the study of an Infrared (IR) optical-based system----MScMS-II (Mobile Spatial coordinate Measuring System-II), which is designed to perform low-cost and easy indoor coordinate measurements. The architecture and working principles of the system are thoroughly described in this chapter and some possible improvements (e.g. a concept design of smart probe involved in the system) are introduced as well.

2.2 Description of MScMS-II system

The MScMS-II system is an indoor coordinate measuring system based on IR optical technology, designed for large-scale metrology applications. The system, developed at Industrial Metrology and Quality Engineering Laboratory of DIGEP-Politecnico di Torino, consists of three basic units (Maurizio Galetto et al. 2010a):

- a network ("constellation") of wireless sensors, opportunely distributed within the measurement volume, to estimate 3D coordinates of reflective passive markers;
- a mobile wireless and armless probe, equipped with two reflective markers, to "touch" the points to be measured, providing capabilities to walk around the object to be measured without being mechanical constraints;
- a data processing system, using Bluetooth connection, to acquire and elaborate data sent by each network sensor.

The architecture of MScMS-II is presented in figure 2-1. The basic units and working principles are described in the following sections respectively.

2.2.1 Sensor network

Currently, a prototype of the distributed network has been set up by using commercial low-cost IR cameras, characterized by an interpolated resolution of 1024 (H) x 768 (V) (native resolution is 128 x 96 pixels, horizontal and vertical respectively), a maximum sample rate of 100 Hz, and a field of view (FOV) of approximately 45°×30°. Each camera implements a real-time multi-object tracking (MOT) engine, which allows tracking up to four IR light sources. In order to work with passive markers, each camera is coupled with a near-IR light source (Fig. 2-2), consisting of a 160-chip LED array with a peak wavelength of 940 nm and a viewing half-angle of approx. 80°. The overall sensor set (camera and LED array) weights about 500 g and is sized 13x13x15 cm. The IR sensor configuration can be set according to shape and size of the measured object as well as of the working environment (Maurizio Galetto et al. 2010b).

Given a fixed number of cameras, all operating conditions being unchanged, the actual working volume, intended as the region within which the spatial position of a single marker

can be reconstructed, depends on the technical specifications of IR cameras (e.g., FOV, sensitivity, pixel resolution, and focal length) and light sources (e.g., LED power and wave length) as well as on the sized of markers. According to triangulation principles, this volume is determined by the intersection of FOV of at least two cameras. It has been noted that a network layout of six commercial low-cost IR sensors, arranged in a 5.0 x 6.0 x 3.0 m^3 working environment according to a grid-based configuration, results in an actual working volume of about 2.0 x 2.0 x 2.0 m^3. Fig. 2-3 provides a virtual reconstruction of the working layout, with reference to a six-camera configuration.

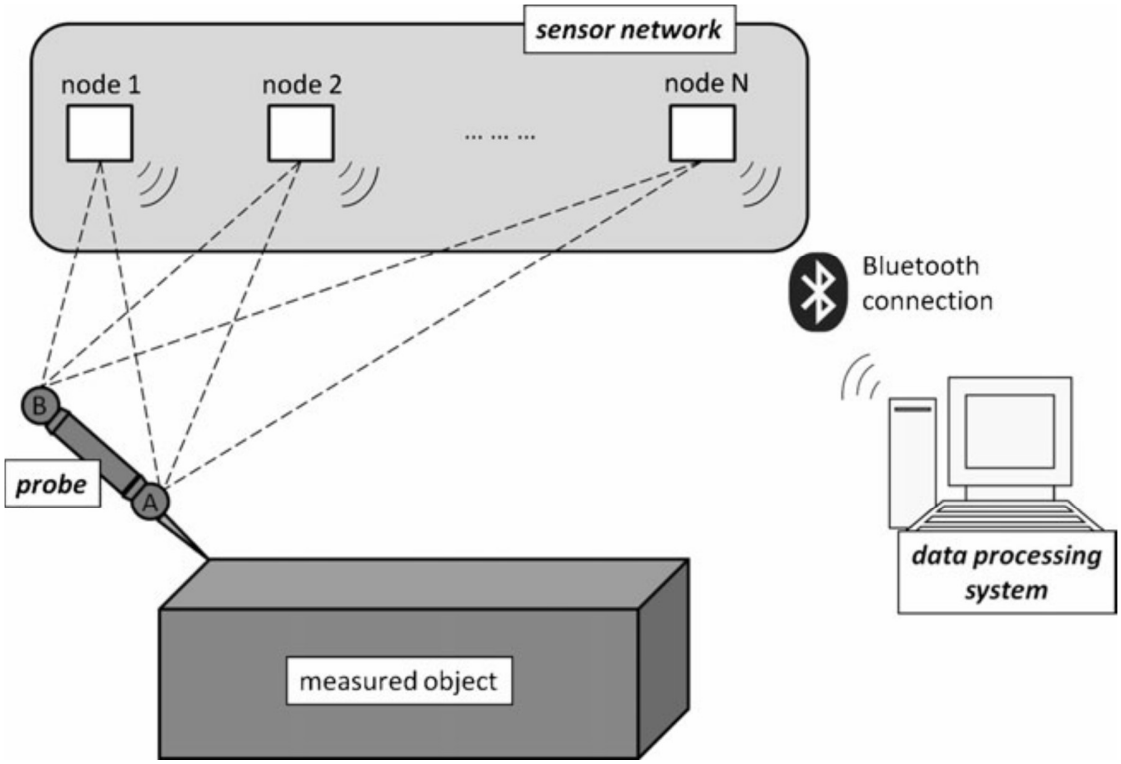

Fig. 2-1 MScMS-II architecture. The dashed lines represent visual links between sensor nodes and retro-reflective spheres (indicated as A and B) equipping the handheld probe. The Bluetooth connection is established between each node and the processing system (Maurizio Galetto et al. 2010a).
(with permission)

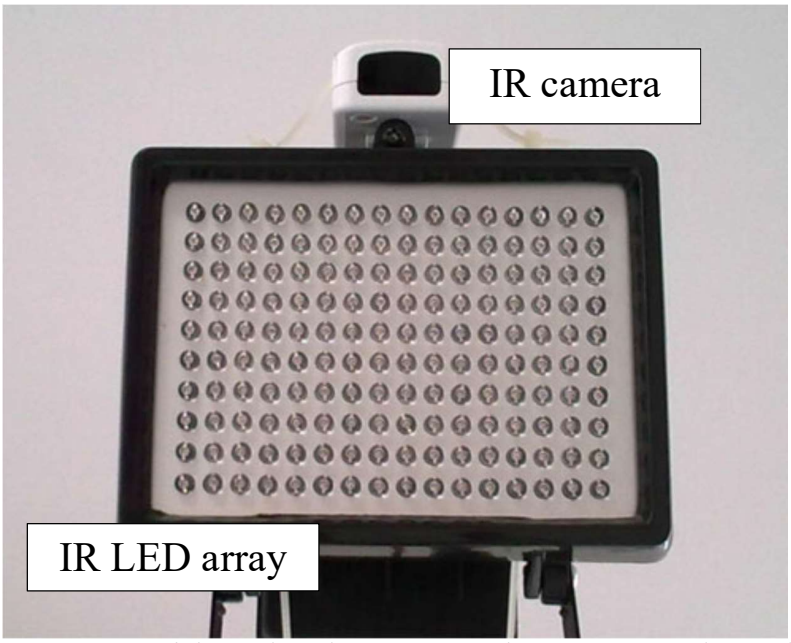

Fig. 2-2 Main components of the IR-based sensor network: an IR camera is coupled with an IR LED array to locate passive retro-reflective targets (Maurizio Galetto et al. 2010a). (with permission)

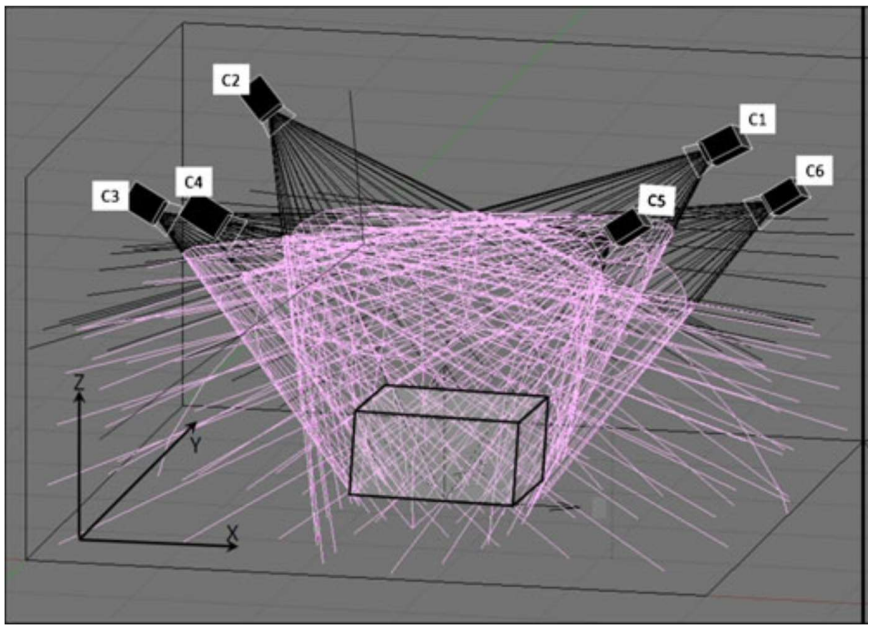

Fig. 2-3 Virtual reconstruction of the working layout. The *black wireframe* represents the camera' FOV, whereas the *light pink wireframe* represents the working volume (interpreted as the volume of intersection of at least two FOV). A 1.5 x 0.8 x 0.5 m^3 box, representing a reference object to be measured, has been placed within the working environment (Maurizio Galetto et al. 2010a). (with permission)

2.2.2 Measuring probe

The mobile probe (Fig. 2-4) consists of a rod, equipped with two reflective markers at the extremes and a stick (stainless steel stick, with ultra-hard ruby ball-tip) at one end to physically "touch" the points to be measured. Passive markers have been made by wrapping around polystyrene spheres a retro-reflective silver transfer film. The marker's dimension depends on hardware capabilities and working volume. The IR camera's sensitivity has been experimentally evaluated by testing visibility distance of differently sized retro-reflective spheres. The implemented technology demonstrated to be able to track a 40-mm diameter marker at a maximum distance of 6 m. It is noteworthy that, due to its lightweight and simple design, the measuring probe could be handheld as well as carried onboard by an autonomous agent (ground or aerial robot) (Maurizio Galetto et al. 2010b), providing up to 6DOF in performing the measurement task.

Referring to Fig. 2-4, as the probe tip (V) lies on the same lien of the centers of the markers (A, B), spatial coordinates of point $X_V \equiv (x_V, y_V, z_V)$ can be univocally determined by the following linear equation:

$$X_V = X_A + \frac{(X_B - X_A)}{\|X_B - X_A\|} \cdot \|X_V - X_A\| \tag{2-1}$$

where $X_A \equiv (x_A, y_A, z_A)$ and $X_B \equiv (x_B, y_B, z_B)$ identify the centers of markers of A and B, respectively. The term $\|\cdot\|$ represents Euclidian distance (Wikipedia), and $\|X_V - X_A\|$ is a priori known as it depends on probe geometry. The so obtained values of $X_V \equiv (x_V, y_V, z_V)$ must be further corrected by the error due to the non-punctiform shape of the tip. To this end a specific algorithm has been implemented in the MScMS-II software (M. Galetto et al. 2010a).

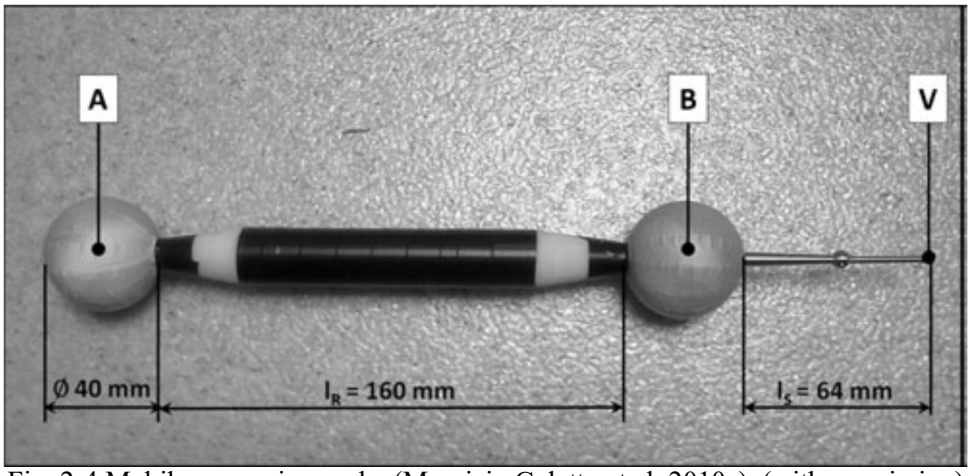

Fig. 2-4 Mobile measuring probe (Maurizio Galetto et al. 2010a). (with permission)

2.2.3 Data processing unit

The data processing hardware consists of a 2.5 GHz computer platform, connected to a set of IR cameras via a Bluetooth link. Each camera provides for the data processing system the 2D coordinates of the IR spot(s) in its view plane. As a matter of fact, the embedded real-time tracking capabilities of the IR sensor save the computational effort for performing the image analysis and spot coordinates identification by the computer platform. As the connection is based on a Bluetooth link, cameras are sequentially sampled. Hence, image synchronization represents a critical issue for 3D reconstruction performance, depending on acquisition delays. According to the hardware-software configuration, a maximum number of six IR sensors can be managed by a single PC unit. A modular approach, based on multiple processing units sharing the information of different camera sets, can be implemented to enlarge the working volumes. Considering that the probe is steadied during measurement, with a configuration of six non-synchronized cameras, and using a sampling rate of 50 Hz, preliminary tests showed that the acquisition delay has a negligible influence on measurement results (Maurizio Galetto et al. 2010a).

2.2.4 Software associated with MScMS-II

The processing software associated with MScMS-II system implements the following functions: (i) layout evaluation, (ii) system calibration, (iii) 3D point localization, and (iv) data elaboration procedure.

The layout evaluation block provides a graphical interpretation of configuration, i.e. sensor spatial distributions within the available volume. This “pre-processing” tool provides for computing and drawing the coverage volume, i.e., the volume covered by at least *n* cameras. Furthermore, it could perform as an offline diagnostic tool, reporting operating conditions that could five rise to possible ambiguities in 2D-3D reconstruction. The analyzed configurations can be either user-defined or algorithm-assisted. A computer-assisted procedure for optimal sensor placement can be used to configure the network layout in order to optimize the system performance (M. Galetto, Pralio B 2010).

According to a given network configuration, the calibration block implements a camera self-location algorithm. Taking as input from the camera tracking engine the 2D position estimates of a single reflective marker (calibration marker), randomly moved in several unknown positions within the working volume, it provides camera positions and orientations as well as camera internal parameters (such as focal length, principal point and lens distortion). Locating a calibrated artifact (calibration square, see Fig. 2-5) positioned within the working volume, it performs camera alignment and scaling to a user-defined coordinate reference system.

These information are then used by the localization algorithm to perform 3D reconstruction of measurement points, according to digital photogrammetry principles (Edward M Mikhail et al. 2001).

The data elaboration software tool has been designed as to accomplish system flexibility, by providing capabilities to perform single-point coordinate measurements, distance measurements, as well as geometric features reconstruction. To this end, functions similar to those implemented by CMM commercial packages have been integrated to support the user in elaborating the measurement data and reconstructing basic geometric features (Theodore H Hopp and Mark S Levenson 1995).

2.2.5 Description of system calibration procedure

The multi-camera calibration problem is faced by using a fully automatic sing-point self-calibration technique (T. Svoboda et al. 2005).

Different from other existing calibration methods (Roger Y Tsai 1987, Zhengyou Zhang 2000), the one applied to MScMS-II system does not require position of a 3D calibration object at known 3D coordinates and is able to reconstruct internal parameters besides positions and orientations of a camera set. Notwithstanding, this extremely flexible, fast, and easy-to-use technique requires a minimum of three cameras as the internal parameters are the same for all cameras, but they are completely unknown. The reference system alignment and scaling procedures are carried out by positioning a calibrated artifact within the working volume. The reference system origin and orientation are thus fixed according to the measurement task and/or the measured object.

According to the calibration procedure, a single reflective marker is randomly moved in several unknown positions within the working volume and tracked by the IR camera sensors. Image acquisition and processing are managed by the camera onboard hardware that directly provides pixel coordinates in the view plane. Modifications to the original MATLAB calibration toolbox in (T. Svoboda) have been made to provide as input pixel coordinates instead of pixel images. As a matter of fact, the camera onboard tracking capabilities save the automatic spot detection procedure, which is a computationally expensive operation. On the other hand, camera self-calibration as well as probe localization is affected by the reliability of the embedded tracking engine, i.e., by its capabilities to correctly identify the bright spot in the image and to calculate its position in the camera view.

Firstly, the calibration algorithm performs a two-step procedure for discarding outliers, either due to reflections in the working environment or measurement errors of the tracking engine. False points are removed from the list of visible points of the IR cameras according to an iterative pair-wise analysis and a 2D reprojection error-based strategy. As to the former step, image pairs are iteratively selected according to the number of visible corresponding points. Point-to-point correspondence is analyzed according to epipolar geometry constraints (HC

Longuet-Higgins 1981, Richard Hartley and Andrew Zisserman 2004) and applying a RANSAC-based technique (Martin A Fischler and Robert C Bolles 1981) for discarding outliers. Survived points are further evaluated by projecting them back to the camera pairs and applying a threshold method based on 2D reprojection errors for removing false ones. Then the calibration algorithm implements an iterative procedure that compute the projective structure (i.e., the projection matrix and the cloud of reconstructed 3D points) until outliers are completely removed and estimate a nonlinear distortion model of the camera lens until a stopping condition (either based on a user-defined threshold or a maximum number of iterations) is reached. Finally, this procedure yields five internal camera parameters (focal length, principal point coordinates, skew coefficient, and radial and tangential distortion coefficients) and six external camera parameters (3D position coordinates of the camera center and orientation angles of its optical axis). As the external camera parameters are provided in an unknown reference frame, having the origin in the center of the cloud of points, a further step for aligning and scaling the world coordinate system is needed. To this end, a laser cut aluminum square (300×400 mm sized), measured to submillimeter accuracy by a CMM, is used as calibrated artifact (see Fig. 2-5).

Fig. 2-5 Reference calibrated artifact, i.e. a laser cut aluminum square (300×400 mm sized).

2.2.6 Localization algorithm

Given a camera layout (i.e. fixed number (n_c) of cameras, with known technical characteristics, positions and orientations, etc.) focused on m markers, for each m-tuple of 2D pixel coordinates $U_{ij} \equiv (u_{ij}, v_{ij})$, with i=1,..,n_c and j=1,…,m, the localization algorithm provides the 3D coordinates of the corresponding m retro-reflective markers (Fig. 2-6). The localization procedure, following the fundamentals of digital photogrammetry, is articulated in two main steps (Maurizio Galetto et al. 2010a):

1 Find the correspondence among pixels in different image views.

2 Match the 2D information of different camera views for recovering the spatial coordinates of the 3D point.

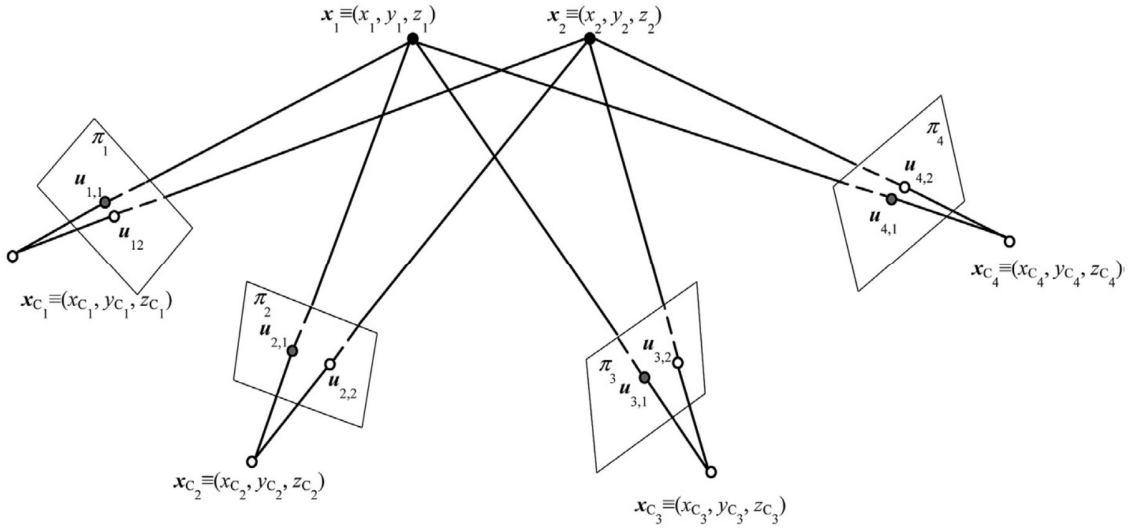

Fig. 2-6 Graphical representation of the localization problem when a setup of four cameras (n_c=4) is used to reconstruct the 3D position of two markers (m=2). X_{Ci} (with i=1,…,4) and X_{Mj} (with j=1,2) refer to the 3D coordinates of the ith camera center and the jth marker, respectively. Point u_{ij} represents the 2D projection of X_{Mj} onto the image plane of the ith camera. It corresponds to the intersection of the camera view plane π_i with the projection line of X_{Mj} (i.e., the line passing through the 3D point and the camera center). (adapted from (Maurizio Galetto et al. 2010a), with permission)

As to the first step, it consists in reconstructing the matrix M of 2D pixel coordinates corresponding to the projection of the same 3D point onto the camera image planes. Since a generic marker j, positioned at unknown 3D coordinates X_{Mj}, might not be visible from all the cameras (e.g., out of FOV, shadowed), $M \in \mathbb{R}^{p\times 2}$where $p \leq n$.

Epipolar geometry, i.e., the intrinsic projective geometry between two views, has been used to correlate information from multiple camera images (HC Longuet-Higgins 1981, Richard Hartley and Andrew Zisserman 2004). The correlation between two 2D pixels, $U(u, v)$ and $U'(u', v')$, detected by two different cameras, states to what extent thy can be considered as the projections of the same 3D point onto the camera image planes. According to epipolar geometry principles, given a pair of images, to a generic point U in the first image corresponds to a line ℓ (i.e., the epipolar line) in the second image (see Fig. 2-7). The epipolar line is defined as the intersection of the image plane of the second camera with the plane passing through the point U and the two camera centers, X_{C1} and X_{C2}, which will also contain the reconstructed 3D point X_M. This line can be drawn whenever the projection matrices of the given pair of cameras are known. The image view of the 3D point in the second image U' will thus line on the epipolar line ℓ. As a matter of fact, the point correspondence ca be found by evaluating the distance between the 2D pixel U' in the second image and the epipolar line corresponding to the 2D pixel U in the first image.

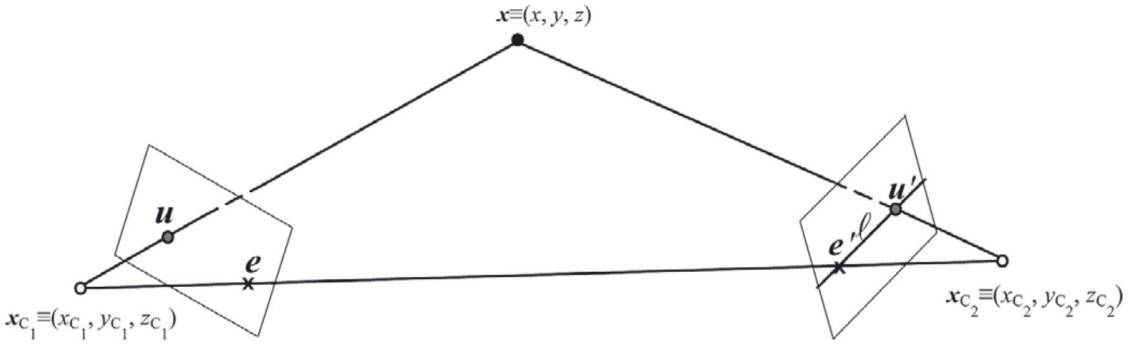

Fig. 2-7 Epipolar geometry principles (Richard Hartley and Andrew Zisserman 2004). X_{C1} and X_{C2} are the camera centers, X_M is the 3D point. *U* and *U'* represent the 2D projection of X_M onto the image planes of the first and second camera, respectively. *e* and *e'* are the epipoles of the two cameras, i.e., the intersection of the line joint the two camera centers with the image plane. *l* is the epipolar line corresponding to *U.* (adapted from (M. Galetto et al. 2010a), with permission)

As the epipolar distance is proportional to the reprojection error after triangulation, large epipolar distances mean pixel correlation mismatches and large projection errors. A threshold method has been implemented to find correspondences between different image views.

The current presence of more than one retro-reflective marker within the working volume could give rise to some ambiguities in measurement point recovery. In some practical cases, probe positioning with respect to the IR sensor and its orientation could correspond to a very small distance between the two pixels in an image view. In order to reduce the errors in pixel correlation, a minimum search approach has been implemented. Stated that two pixels *U'* and *U''* in the second camera view verified the threshold constraints, the point *U* in the first camera view will be correlated to the one having the minimum epipolar distance to its epipolar line ℓ.

The second step of the localization algorithm deals with the triangulation problem (Richard I Hartley and Peter Sturm 1997). Given its 2D positions in *n* different image planes (with $2 \leq n \leq n_c$), the 3D coordinates of a point X_M can be obtained by intersecting the camera projection lines (triangulation). Hence, the set of $2 \times n$ equations with unknown variables (x_M, y_M, z_M) can be written as:

$$AX_M - B = 0 \tag{2-2}$$

Where $A \in \mathbb{R}^{2n\times 3}$ and $B \in \mathbb{R}^{2n\times 1}$ are known matrices, whose elements are obtained as functions of camera projection matrices and 2D pixel spatial coordinates $U_i(u, v)$ (with $i=1,\ldots,n$).

In practical applications, due to measurement noise and sensor hardware limits, the projection lines do not generally meet in a unique point, and a least-squares minimization is needed using two or more cameras. To this end, a single value decomposition method (Gene H Golub and Christian Reinsch 1970) has been chosen to solve Eq. 2-2 for X_M, obtaining an

approximated vector of position coordinates X^*_M. According to the vector of residual $E \equiv AX^*_M - B$, a parameter e, directly proportional to the overall variance, is estimated as (Fiorenzo Franceschini et al. 2009):

$$e \propto E^T E \tag{2-3}$$

This parameter is used as preliminary diagnostics in order evaluate the correctness of 3D positioning. The estimated coordinates $X^*_M(x^*_M, y^*_M, z^*_M)$ of the measured point, if characterized by a high variance values, are automatically discarded according to a threshold method.

It has to be noted that, as they are based on the 2D image views of different cameras, the triangulation results strongly affected by camera synchronization issues. As a matter of fact, the 3D point reconstruction algorithm should use the 2D pixel coordinates of the same point as seen by the different cameras sensors at the same time instant (synchronized camera sampling). Whenever a sequential sampling procedure is implemented, the higher is the number of sensors the higher is the total acquisition delay and thus possible discrepancies among different image views. Whereas it could represent a problem for tracking dynamic objects, sequential sampling has negligible influence on measurement performance as data acquisition is made by keeping the probe in stable position.

2.2.7 Summary of MScMS-II system

A preliminary test has been conducted by (Maurizio Galetto et al. 2010a), in order to investigate the performance (e.g., stability, repeatability, and reproducibility) of the overall system. Specifically, the test configuration is summarized as follows:

- a set of six IR cameras is arranged in a grid-based layout in the working environment;
- the measurement volume is about 2.0×2.0×2.0 m^3;
- a sampling frequency of 50 Hz is used for data acquisition.

The stability (i.e., the property of a measuring instrument, whereby its metrological properties remain constant in time (IEC BIPM et al. 2008)) test has been designed to measure s=15 different positions that are distributed all over the measurement volume, by replicating the measurement k=30 times (over a span of time of approx. 300 seconds) for each position. The standard deviation of measured 3D coordinates has been estimated, which is a measure of the system stability, i.e., the lower is the variance, the higher stability the system has, the test results are shown in table 2-1.

The repeatability (i.e., "closeness of the agreement between the results of successive measurements of the same measurand carried out under the same conditions of measurement" (IEC BIPM et al. 2008)) has been tested on s=5 different points, uniformly distributed within the measurement volume. The test is carried out by repeating the measurement k=30 times for each point, repositioning the probe in the same positions for each measurement, results

of repeatability tests are reported in table 2-2, in terms of sample mean and standard deviation of the reconstructed 3D positions of the probe tip V.

Measurement reproducibility, intended as "closeness of the agreement between the results of successive measurements of the same measurand carried out under changed conditions of measurement" (IEC BIPM et al. 2008), has been tested with reference s=5 points, distributed all over the measurement volume. For each point, the measurements have been repeated k=30 times with different angular orientations of the mobile probe. Table 2-3 reports the statistical results of these preliminary test. As expected, the standard deviation is basically higher for reproducibility tests. This behavior can be basically ascribed to the strong influence the relative position and orientation of probe and network devices has on overall measurement accuracy.

Table 2-1 Mean and standard deviation results for stability preliminary tests. The sample mean values refer to a user-defined room-aligned reference coordinate system.

	$\overline{x}$ [mm]	$\overline{y}$ [mm]	$\overline{z}$ [mm]	$\hat{\sigma}_X$ [mm]	$\hat{\sigma}_Y$ [mm]	$\hat{\sigma}_Z$ [mm]
Point 1	-207.20	-300.35	-83.98	0.18	0.16	0.18
Point 2	-146.9	163.49	-75.87	0.33	0.18	0.22
Point 3	65.29	-40.32	-77.23	0.15	0.28	0.34
Point 4	330.53	329.98	-72.17	0.27	0.24	0.30
Point 5	330.31	-357.60	-74.51	0.14	0.10	0.21
Point 6	257.63	228.29	391.59	0.12	0.31	0.15
Point 7	249.58	-277.87	383.17	0.11	0.17	0.08
Point 8	-193.08	-304.65	392.24	0.39	0.28	0.32
Point 9	-232.05	193.58	397.85	0.15	0.10	0.20
Point 10	15.80	15.20	386.91	0.16	0.09	0.17
Point 11	-221.98	138.48	529.86	0.25	0.13	0.11
Point 12	-172.10	-288.12	520.14	0.29	0.15	0.35
Point 13	0.77	-36.05	514.68	0.14	0.14	0.13
Point 14	250.14	139.75	523.14	0.15	0.15	0.13
Point 15	85.84	-45.91	514.43	0.29	0.38	0.23

Table 2-2 Mean and standard deviation results for repeatability preliminary tests. The sample mean values refer to a user-defined room-aligned reference coordinate system.

	$\overline{x}$ [mm]	$\overline{y}$ [mm]	$\overline{z}$ [mm]	$\hat{\sigma}_X$ [mm]	$\hat{\sigma}_Y$ [mm]	$\hat{\sigma}_Z$ [mm]
Point 1	-179.56	-188.55	-41.99	1.25	0.75	0.69
Point 2	257.70	135.87	-28.46	0.79	0.61	0.36
Point 3	-159.09	182.61	-36.57	0.45	0.43	0.39
Point 4	171.66	-238.84	-29.08	0.61	0.89	0.55
Point 5	-13.92	-23.52	-35.56	0.31	0.34	0.27

Table 2-3 Mean and standard deviation results for reproducibility preliminary tests. The sample mean values refer to a user-defined room-aligned reference coordinate system.

	$\overline{x}$ [mm]	$\overline{y}$ [mm]	$\overline{z}$ [mm]	$\hat{\sigma}_X$ [mm]	$\hat{\sigma}_Y$ [mm]	$\hat{\sigma}_Z$ [mm]
Point 1	176.77	333.15	277.87	2.49	1.76	1.54
Point 2	224.39	-70.61	276.91	1.67	0.66	1.21
Point 3	-206.23	-107.96	265.66	2.54	1.03	1.80
Point 4	-258.53	409.44	266.44	3.45	2.10	2.05
Point 5	11.91	141.64	278.28	2.42	0.83	2.43

According to a preliminary test conducted by (Maurizio Galetto et al. 2010a), the MScMS-II prototype does not provide competitive performance with respect to available commercial systems such as CMMs, laser trackers, iGPS, etc. Those technologies, in the same working volume, are characterized by a measurement uncertainty ranging from few micrometers up to 1 mm at worst, depending on the system, the working conditions and the measurement procedure (F. Franceschini et al. 2009, D. A. Maisano et al. 2009). However, the experimental results become particularly interesting if cost and potentiality of the metrological system are considered. Whereas its distributed architecture ensures scalability and flexibility that exiting commercial systems cannot guarantee, the prototype still has significant room for improvement mainly related to the sensing technology. An improvement of the network hardware could provide a considerable increase (one order of magnitude at least) in system accuracy, by implementing commercial optical technologies with a limited impact on the cost of the entire system (Maurizio Galetto et al. 2010a).

In a research perspective, a closer examination of factors affecting system performance, including IR hardware characteristics (e.g. sensor resolution and sensitivity), camera synchronization, self-calibration, and localization algorithms, is worthy carrying out. Further investigation should be devoted to the effects of the calibration and scaling procedures and to possible correction models for decreasing the average error.

2.3 New design of a smart probe

The contact probe (see Fig. 2-4) used in MScMS-II system has a simple design that consists of (i) a slim rod which is easy to be held by human and/or robot arm; (ii) two retro-reflective markers that is able to be recognized by IR cameras, whenever they are illuminated in the FOV; (iii) a stainless steel stick with ultra-hard ruby ball-tip that is used to touch the object to be measured. The coordinates of ball-tip can be determined by localizing the two markers in 3D space and knowing the geometry of the probe (i.e., the distance between two markers and that between the tip and markers). In order that the markers can be detected by the distributed sensors, there must be an external light sources (e.g. the IR LED array adopted in the sensor network of MScMS-II, see Fig 2-2). However, when the working environment or the objects to be measured are highly reflective, the external light sources may cause high ambiguities in detection of markers by IR sensors. Besides, in practical applications, the environmental conditions cannot always be controllable (e.g. applications outside Laboratory environment), such as temperature, humidity, lighting condition, those environmental conditions have strong influence on the optical-based sensors, especially in large-sized working volume.

2.3.1 Concept design of new probe

The new design of the contact probe, named “smart probe”, has been developed in order to enrich the functions of current probe (Fig. 2-4) in many aspects:

(i) it does not require an external light source, but can illuminate markers by internal light sources, which eliminates the reflection caused by external light source;
(ii) it integrates many sensors (e.g. accelerometer, gyroscope, thermometer, humidity sensor, etc.) to monitor kinematic variations and/or environmental conditions during the measurement, which allows to correct and compensate the measurement results based on parameters of external influence;
(iii) it is equipped with antenna for wireless communication and sensors’ data transfer to DPU.

The scheme of new design of probe is illustrated in Fig. 2-8, where the description and function of each component are described in table 2-4.

The invention of smart probe has been registered and protected by the Italian Patent and Trademark Office (Fiorenzo Franceschini et al. 2016).

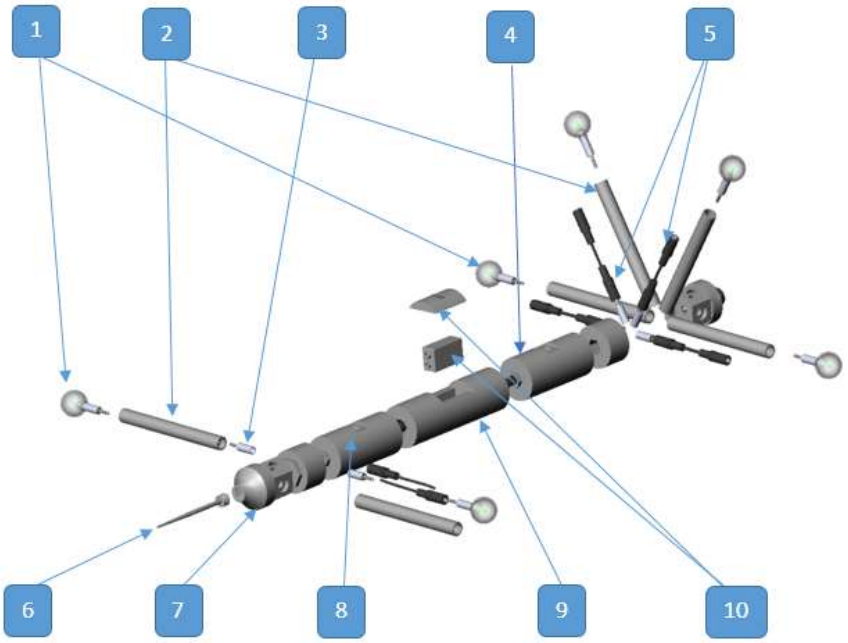

Fig. 2-8 The scheme of new design of probe.

Table 2-4 Description of components of new design of probe.

Component No.	Description	Function
#1	Active marker	Translucent polymer spherical marker with internal IR light source.
#2	Tube	Opaque and rigid tube housing wires.
#3	Connection port	Magnetic connection port.
#4	Antenna	Antenna for wireless communication with DPU.
#5	Cable	Cables connecting markers and power supply.
#6	Tip	The stainless steel stick with ultra-hard ruby ball-tip for touching the object to be measured.
#7	Hub	Connection hub for plug-in markers.
#8	Trigger	Trigger button for data acquisition.
#9	Rod	Body for handling and socket for battery and sensors.
#10	Battery and cover	Power supply and socket cover.

2.3.2 Prototype of new probe with active markers

The new design of contact probe, characterized by its use of "active markers" (i.e., spherical markers illuminated by internal light sources), can emit light of wavelength in infrared range and/or visible light range, corresponding to IR sensor network and/or generic CCD sensor network, respectively. The active marker is composed of an LED and a translucent polymer sphere of diameter 40 mm, and the latter can uniformly diffuse the LED light, in order to obtain a spherical marker that is uniformly illuminated in the working environment. The sketch and prototype of an active marker is shown in Fig. 2-9.

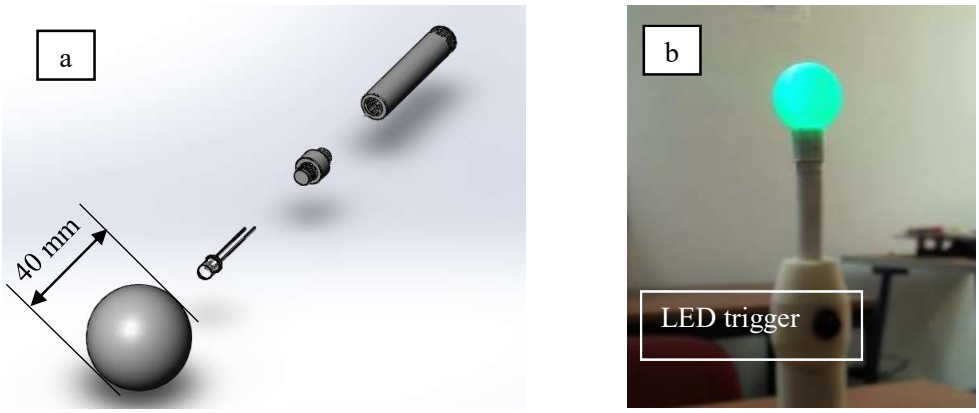

Fig. 2-9 (a) Sketch of an active marker. (b) Prototype of an active marker (with green light).

A prototype of new probe with four active markers has been developed by 3D printing technique (see Fig. 2-10), in order to verify the camera system can function properly with active markers. It is noteworthy on two aspects: (i) the diameter of active markers equals to 40 mm, aiming at imitating the same geometry of passive markers; (ii) localization of probe tip is more complicated than that of the current one, since the new probe has employed more markers (redundancy in markers) and formed a nonlinear shape. The localization issue is discussed in next section.

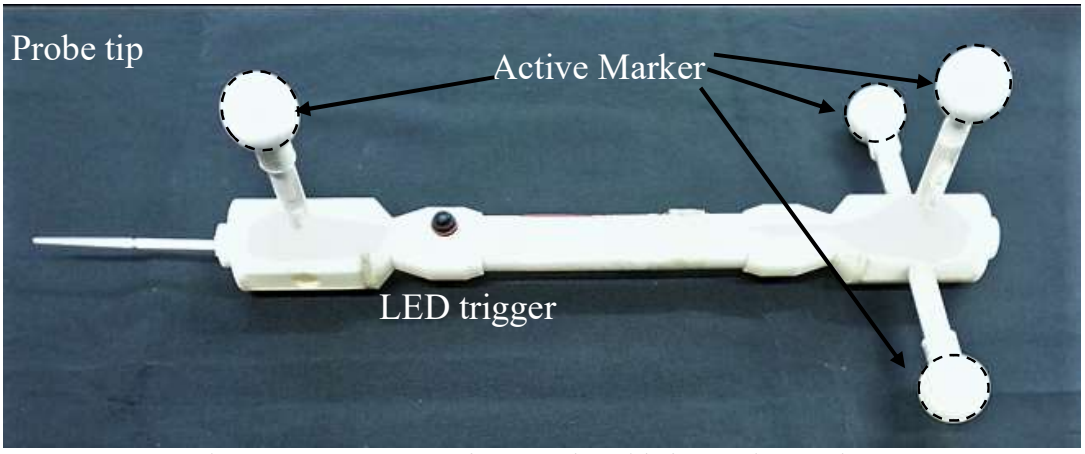

Fig. 2-10 A prototype of new probe with four active markers.

2.3.3 Localization of new probe tip

The localization issue of new probe tip is faced with Procrustes algorithm (John C Gower and Garmt B Dijksterhuis 2004). Localization of a single marker is solved by triangulation method, i.e., the 3D coordinates of one marker can be determined whenever it is in the FOV of at least two sensors of the network. Once a number of markers (at least 3, with non collinear topology) have been localized in the working volume, the 3D coordinates of the point touched by the tip can be derived by knowing the relative positions between the tip and markers, which have been calibrated before doing measurement, by a measuring instrument with higher accuracy, like CMM. The calibrated result is stored as a database for the following tip localization, and it is noteworthy that, calibration is required whenever the tip and/or markers are changed.

The coordinates of markers measured by MScMS-II are compared to those measured by CMM (the database), by applying Procrustes algorithm. Procrustes algorithm outputs a linear transformation matrix (defining rotation, translation and scaling factor) of the points in one matrix to best conform them to the points in another matrix. The goodness-of-fit criterion is the sum of squared errors, which is as well a measure of overall accuracy of point measurement by MScMS-II. The transformation matrix is then applied to the coordinates of tip measured by CMM to obtain the coordinates of tip measured by MScMS-II.

3. Error correction methods for MScMS-II

3.1 Introduction

MScMS-II is a prototype system designed for large scale metrology applications. It is characterized by a distributed modular architecture, consisting of a network of wireless sensors, which are capable of real-time tracking IR spot(s) in the camera view plane by MOT engine. The working principle of transforming 2D pixel coordinates in image plane of sensors into 3D reconstructed points in measuring volume is the well-known triangulation-based photogrammetry. Due to its architecture and working principle, the system is affected by several systematic error sources. Some of them are addressed in this chapter: the distortion of each camera lens, the dimension of the probe tip, the kinematic of the probe and the imperfect determination of the system calibration parameters.

This chapter presents the study of a set of corrective algorithms for measurement improvement in MScMS-II system and by means of the implementation of appropriate mathematical correction models, the overall system performance is significantly improved, as shown in the conducted tests.

3.2 Lens distortion correction

Radial (symmetric) distortion constitutes the major imaging error for most camera systems. It is attributable to variations in refraction at each individual component lens within the objective. It is a function not only of the lens design used but also of the chosen focusing distance, and of the object distance at a constant focus. Fig. 3-1 shows the effect of radial distortion as functions of the image radius of an imaged point. In the example, the radial distortion increases with the distance from the principal point. Brown (C BROWN Duane 1971) shows that the distortion curve can be modeled with polynomial series (Seidel series) with distortion parameters k_i, i=0,…,n:

$$\begin{aligned} \Delta u_{rad} &= u(k_1 r^2 + k_2 r^4 + k_3 r^6 + \cdots) \\ \Delta v_{rad} &= v(k_1 r^2 + k_2 r^4 + k_3 r^6 + \cdots) \end{aligned} \tag{3-1}$$

where (u, v) are the normalized pixel coordinates of a camera and $r = \sqrt{u^2 + v^2}$ (C BROWN Duane 1971).For most lens types the series can be truncated after the second or third term without any significant loss of accuracy.

Radial-asymmetric distortion, often called tangential or decentering distortion (Fig. 3-1), is another important imaging error, which is mainly caused by lack of concentricity and misalignment of individual lens elements within the objective. It can be compensated by the following function (C BROWN Duane 1971):

$$\Delta u_{tan} = b_1(r^2 + 2u^2) + 2b_2uv$$
$$\Delta v_{tan} = b_2(r^2 + 2u^2) + 2b_1uv \tag{3-2}$$

Where b_1 and b_2 are tangential distortion coefficients. Compared to the radial-symmetric part, radial-asymmetric distortion shows much smaller values for most quality lenses (Zhengyou Zhang 1999). Hence, it is often determined for high accuracy specifications only. In case of low cost lenses, significant tangential distortion can be found. For this reason, it is reasonable to expect a significant improvement in the performance of MScMS-II from the implementation of correction model for both radial and tangential distortion. The complete correction model can be stated as:

$$u_{corrected} = u + \Delta u_{rad} + \Delta u_{tan}$$
$$v_{corrected} = v + \Delta v_{rad} + \Delta v_{tan} \tag{3-3}$$

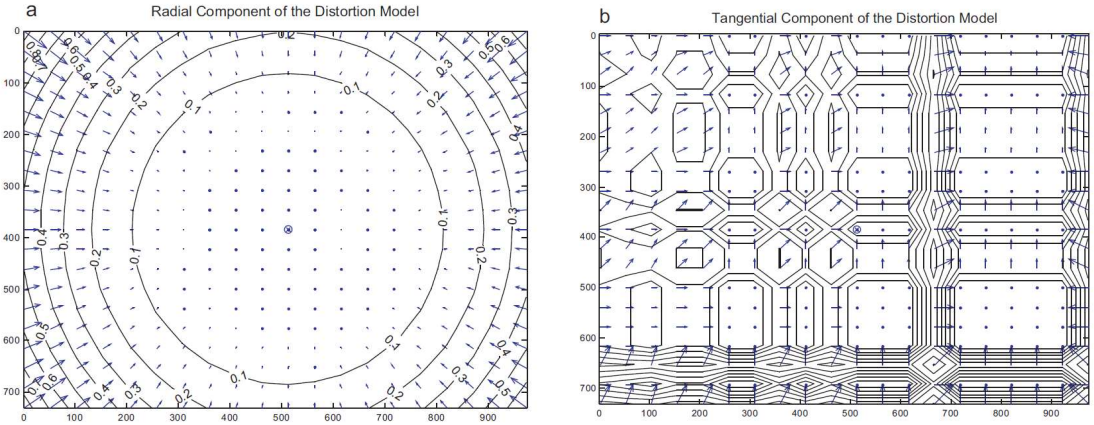

Fig. 3-1 Lens distortion. (a) Example of lens radial distortion (b) example of lens tangential distortion.

Fig. 3-1 represents an example of lens distortion correction. For each region of the image, the arrows indicate the direction and the magnitude of vectors ($\Delta u_{rad}, \Delta v_{rad}$) and ($\Delta u_{tan}, \Delta v_{tan}$) respectively.

The effectiveness of the presented model is verified by the following performed test (Maurizio Galetto and Luca Mastrogiacomo 2013). A reference artifact was calibrated using a coordinate measuring machine whose nominal accuracy is of the order of a hundredth of a millimeter (CMM-DEA Iota0101). The reference artifact used for measurement is introduced in Fig. 2-5. On the artifact four different reference distances about 100, 200, 400 and 500 mm were defined. The reference artifact was then measured in three different positions within the measuring volume of MScMS-II. For each position of the reference artifact, the distances were measured with MScMS-II, replicating the measurements 10 times (for a total of 120 measurements). The results of these measurements with and without the correction of lens distortion were compared in terms of deviation from nominal values. As expected, the

performance of the system seems to improve with the distortion correction (see Fig. 3-2). The improvement is significant both in terms of bias and in terms of dispersion of the error distribution.

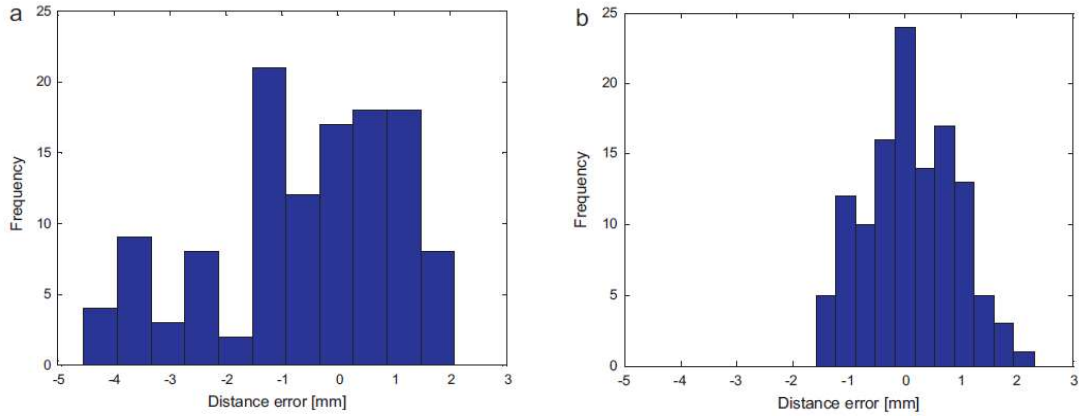

Fig. 3-2 The effect of lens distortion correction. (a) Results of raw measurements (b) results of corrected measurements. (adapted from (Maurizio Galetto and Luca Mastrogiacomo 2013), with permission)

A remarkable aspect that emerges from the proposed tests is how the correction model changed the shape of the error distribution. The shape of the empirical distribution of corrected measurements shows to be much more symmetrical than the uncorrected one. Similar results was obtained in the repeated tests with the same and with different sensor locations, which verifies the robustness of the obtained results (Maurizio Galetto and Luca Mastrogiacomo 2013).

These results justify the choice of this type of camera: despite the low resolution (native 128x96 pixels) the dispersion of the localization results is relatively low and comparable to what could be achieved with cameras with higher resolution (640x480) which have significantly higher costs. Consider that the cost of an industrial camera with VGA resolution is currently higher than 400€, while the cost of the sensors used in the prototype is about 40€ each.

3.3 Bias due to the dimension of the probe

A problem common to all contact measuring instruments is the size of the tip of the probe which may introduce a bias in the contact measurement. For this reason, CMMs software typically implement some algorithms able to correct the measurement results taking into consideration the approaching direction of the probe and the surface shape to be measured (A Woźniak et al. 2009). The stylus tip radius correction (see Fig. 3-3) is an offset vector of norm equal to the effective stylus tip radius which is added to the indicated measured point (i.e. the measured stylus tip center point) to estimate the actual contact or measured point on the profile (i.e. the stylus tip contact point on the actual surface). The nature of the tangential

contact between a sphere and a surface results in the offset vector being normal to the surface at the point of contact so the primary task for correction is to estimate this vector for each data point (Maurizio Galetto and Luca Mastrogiacomo 2013). In the case of a freeform surface or for a contour, the measuring surface normal vector can be unknown especially when dealing with measurements of tight radii, corners or discontinuities in general. A number of approaches have been proposed for solving this problem (A Woźniak et al. 2009).

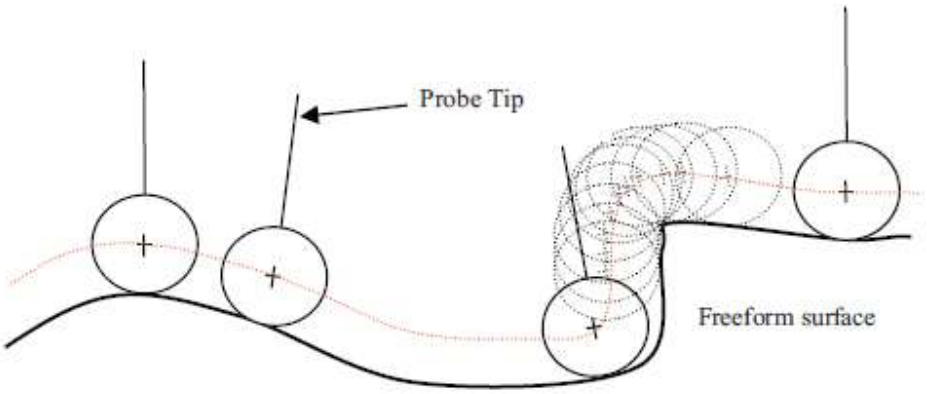

Fig. 3-3 A schematization of the stylus tip approach to a free form. The dotted line represents the envelop of the points measured by the CMM which do not exactly correspond to the surface to be measured. This is particular evident in case of angular points.

Many methods use a set of measured points to estimate the direction of correction. Most of the methods use NURBS (Non-uniform rational B-spline) or cubic splines to obtain a best fit curve through the measured point and its normal vectors in order to compensate as a post-measurement operation (Yin Zhongwei et al. 2003). Another solution assumes that in the neighborhood of the measure point, the surface may approximated by a quadratic equation (C-K Song and S-W Kim 1997). Mayer et al. also used the measured points to fit the surface generated by the stylus tip center and then finding the corresponding normal vector (JRR Mayer et al. 1997). On the other hand, Xiong and Li affirm that since the contact points are on the offset profile of the workpiece, they can use objective function formulated as a least squares problem (Zhenhua Xiong and Zexiang Li 2003). Lin and Sun investigated the stylus tip radius correction using the multi-cross-product method (YC Lin and WI Sun 2003). Another approach for stylus tip radius correction has been based on the use of the part CAD model. Some techniques rely on building a parametric surface or contours followed by the creation of an offset surface using the least squares method (J Jeong and K Kim 1999). Liang and Lin developed a point data conversion algorithm to find the estimated surface normal vector at every point without reconstruction of the surface model (Shuh-Ren Liang and Alan C Lin 2002). They connect surrounding points and on this basis formulate triangular meshes directly from the dense data points set, thus as to determine the normal vector of each point for stylus tip radius correction. Park et al. proposed a probe with an internal elastic structure

fitted with strain gauges so that the contact force between the tip and the measured surface can be estimated and used for the calculation of the stylus tip correction vector (Jae-jun Park et al. 2006). Aoyama et al. proposed a potentiometric spherical tip capable of detecting the point of contact with an electrically conducting object surface (Hideki Aoyama et al. 1989). Without going into details of the case of freeform surfaces, the technical implementation of error compensation in case of areas sections of a known geometric primitive such as a plane, circle, sphere, cone, torus, etc., on MScMS-II was proposed by (Maurizio Galetto and Luca Mastrogiacomo 2013). With MScMS-II, this correction is negligible if using a sharp tip. This type of probe, however, has several drawbacks that limit its use:

- it is not able to make measurements approaching the piece sideways;
- it may introduce a geometrical error due to the imperfections of the tip;
- it introduces a risk of damage to the object to be measured.

From the practical point of view, the procedure implemented for MScMS-II follows the following steps:

- Specification of the target geometry. During this phase the system user is asked to specify the geometry of the surface to be measured.
- Measurement. In this phase a certain number of points P'_i are acquired by means of the portable probe.
- Reconstruction of the envelop. Knowing the specified geometry of the surface, the system computes the envelop interpolating the points P'_i.
- Calculation of the touched points. Knowing the radius of the tip of the probe, the position of the center of the probe tip P'_i and the surface normal $\vec{n}_i$, the generic contact point P_i can be obtained through the relation:

$$P_i = P'_i \pm \vec{n}_i \rho \tag{3-4}$$

The operator sign depends on the direction of the approach of the probe. As an example, consider the simple case of estimating a two-dimensional geometry: a circumference. When measuring a circumference, the envelop of points corresponds to another circle, with the same center but different radius (see Fig. 3-4). The radius depends on the measurement procedure: if the measurement is made approaching the circumference from the outside (outside diameter) the radius will be greater than the real one and vice versa if the measurement is made from within (inside diameter).

During the third step of procedure described above, thee system is able to calculate the geometry of the envelop points P'_i. Being a circumference, the radius ρ' and the center x_0 of the envelop are calculated.

So far, for each point of the envelop, the normal vector can be calculated as:

$$\vec{n}_i = \frac{x_0 - P_i}{\rho} \tag{3-5}$$

Knowing the normal vector, the contact points P_i can be easily calculated by Eq. 3-4. It is noteworthy that, in the example shown in Fig. 3-4, the sign in Eq. 3-4 must be chosen positive, it would have been negative in case of a measurement made with the probe approaching the circumference from the inside.

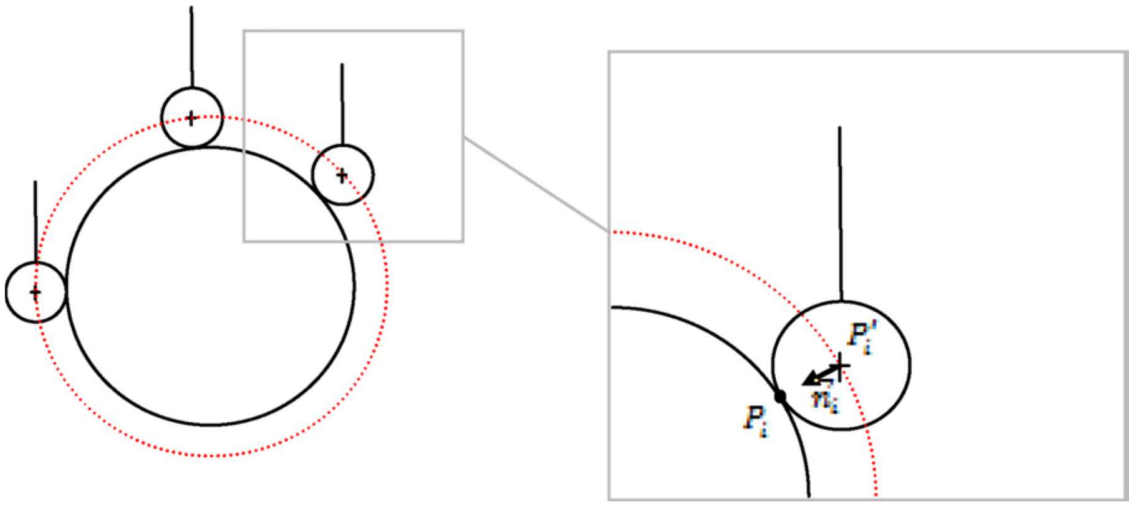

Fig. 3-4 A schematization of the stylus tip approach to a circumference. The dotted line represents the envelop of the points measured by the CMM which, in the particular case, corresponds to a circumference with a different radius. (adapted from (Maurizio Galetto and Luca Mastrogiacomo 2013), with permission)

To make explicit the extent of the improvement deriving from the implementation of the correction model described above, the following test was conducted. A section of a cylinder calibrated with a CMM (DEA Iota0101) was measured with the MScMS-II. The measurement was repeated 30 times in different locations within the working volume of MScMS-II (G. N. Peggs et al. 2009).

The results of the measured with and without correction model were compared with each other (see Fig. 3-5). The nominal value of the radius of the cylinder section was obtained by calibration.

If compared to the nominal value of the diameter of the cylinder section (d=120.00 mm), the results presented in Fig. 3-5 show a bias in the measurement of b=0.98 mm that, as expected, is about half the size of the tip of MScMS-II probe (2 mm). This bias reduces to 0.02 mm when the measurement is corrected considering the size of the probe tip.

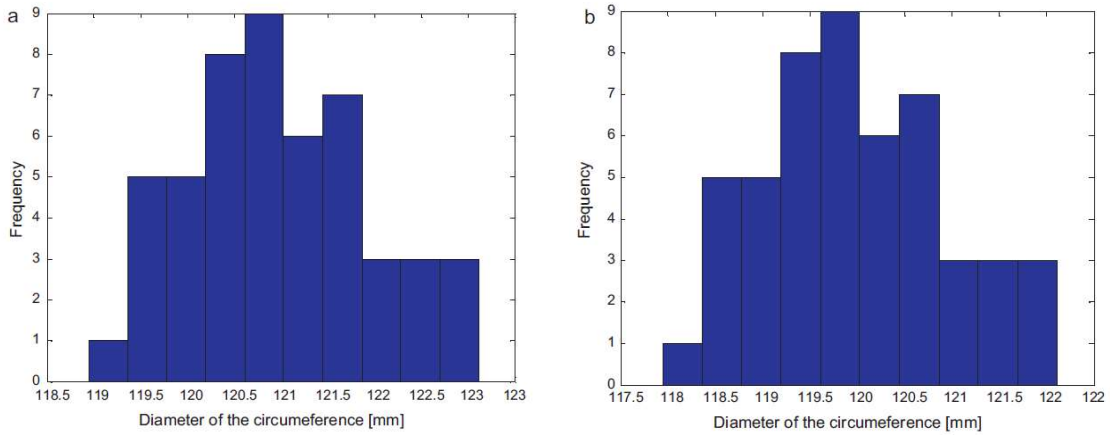

Fig. 3-5 Results of the measurement of the diameter of a cylinder with (a) and without (b) the tip radius correction.

3.4 Bias due to the kinematic of the probe

One of the most well-know and often-used mathematical tools used for stochastic estimation from noisy sensor measurements is the Kalman filter. The Kalman filter is named after Rudolph E, Kalman, who in 1960, published his famous paper describing a recursive solution to the discrete-data linear filtering problem (Rudolph Emil Kalman 1960). The Kalman filter is essentially a set of mathematical equations that implement a predictor-corrector type estimator that is optimal in the sense that it minimizes the estimated error covariance-when some presumed conditions are met (Rudolph Emil Kalman 1960). One of the assumptions for the application of the Kalman filter is the knowledge of the measurement process.

When measuring using the MScMS-II, the operator has to bring the probe in contact with object being measured. At this point, he presses the trigger to take measurements. Although fast enough, this operation is not instantaneous. At a time when the trigger is pressed, the system collects a sample of measurement replications for a fraction of a second (less than one third of a second). During this period, the position of the tip of the probe is supposed to be stationary. For this reasons, the equations that describe this process are:

$$x_k = x_{k-1} + s_k \tag{3-6}$$

with a measurement $z \in \mathbb{R}^3$ that is

$$z_k = x_k + t_k \tag{3-7}$$

where $x_k \in \mathbb{R}^3$ is the position of the probe tip at time k and the random variables $s_k \in \mathbb{R}^3$ and $t_k \in \mathbb{R}^3$ represent the process and measurement noise. They assumed to be independent (of each other), white, and with normal probability distributions:

$$p(s) \sim N_3(0, Q)$$
$$p(t) \sim N_3(0, R) \tag{3-8}$$

where Q and R are respectively the process noise covariance and the measurement noise covariance matrices. Although they could potentially vary in time, they are assumed to be constant in time.

The time update equations are:

$$\hat{x}_k^- = \hat{x}_{k-1}^-$$
$$P_k^- = P_{k-1}^- + Q \tag{3-9}$$

where P_k^- and P_{k-1}^- are respectively the *a prior* estimates of error covariance at time step k and k-1 and $\hat{x}_k^-$ and $\hat{x}_{k-1}^-$ are respectively the *a prior* state estimates at time step k and k-1. On the other hand, the measurement update equations are:

$$K_k = P_k^-(P_k^- + R)^{-1}$$
$$\hat{x}_k = \hat{x}_k^- + K_k(z_k - \hat{x}_k^-) \tag{3-10}$$
$$P_k = (1 - K_k)P_k^-$$

where P_k is the *a posteriori* estimate of the error covariance, $\hat{x}_k$ is the *a posteriori* state estimate at time step k, K_k is the gain that minimizes the *a posteriori* error covariance at step k (Greg Welch and Gary Bishop 2006).

Presuming a very small process variance, it is possible to assume:

$$Q = \begin{pmatrix} 1e^{-5} & 0 & 0 \\ 0 & 1e^{-5} & 0 \\ 0 & 0 & 1e^{-5} \end{pmatrix} \tag{3-11}$$

Assuming a small but non-zero value for Q gives more flexibility in "tuning" the filter (Rudolph Emil Kalman 1960, Greg Welch and Gary Bishop 2006). The filter is "seed" with the guess $\hat{x}_{k-1}^- = x_0$. Similarly the initial value for P_{k-1}, call it P_0 is set as:

$$P_0 = \begin{pmatrix} 1 & 0 & 0 \\ 0 & 1 & 0 \\ 0 & 0 & 1 \end{pmatrix} \tag{3-12}$$

Basing on preliminary empirical tests of measurement accuracy reported by (M. Galetto et al. 2010a, M. Galetto et al. 2010b), the measurement error variance is fixed at:

$$R = \begin{pmatrix} 1 & 0 & 0 \\ 0 & 1 & 0 \\ 0 & 0 & 1 \end{pmatrix} \tag{3-13}$$

In order to provide an idea of the effect of the implementation of this filter, a simple test was designed. In normal operation conditions, the measurement of the position of the probe tip is the result of the acquisition of approximately thirty repetitions of measurement. The system, in fact, has a capture rate that ensures, under these assumptions, an acquisition time of less than 3 tenths of a second. During this period the operator is supposed to keep the probe tip reasonably still.

To give evidence of the effect of the implementation of the filter, 300 repetitions of measurement were recorded keeping the probe still for about 3 s. Fig. 3-6 shows, on the same graph, the measurement with and without the implementation of the filter. From the plot, there is evidence of the fact that the filtered measurements are much more stable than the unfiltered ones. Considering the first 30 observations, the variability of filtered data is respectively σ_x=0.07 mm, σ_y=0.04 mm and σ_z=0.09 mm. On the other hand, the variability of unfiltered data is respectively σ_x=0.35 mm, σ_y=0.13 mm and σ_z=0.29mm.

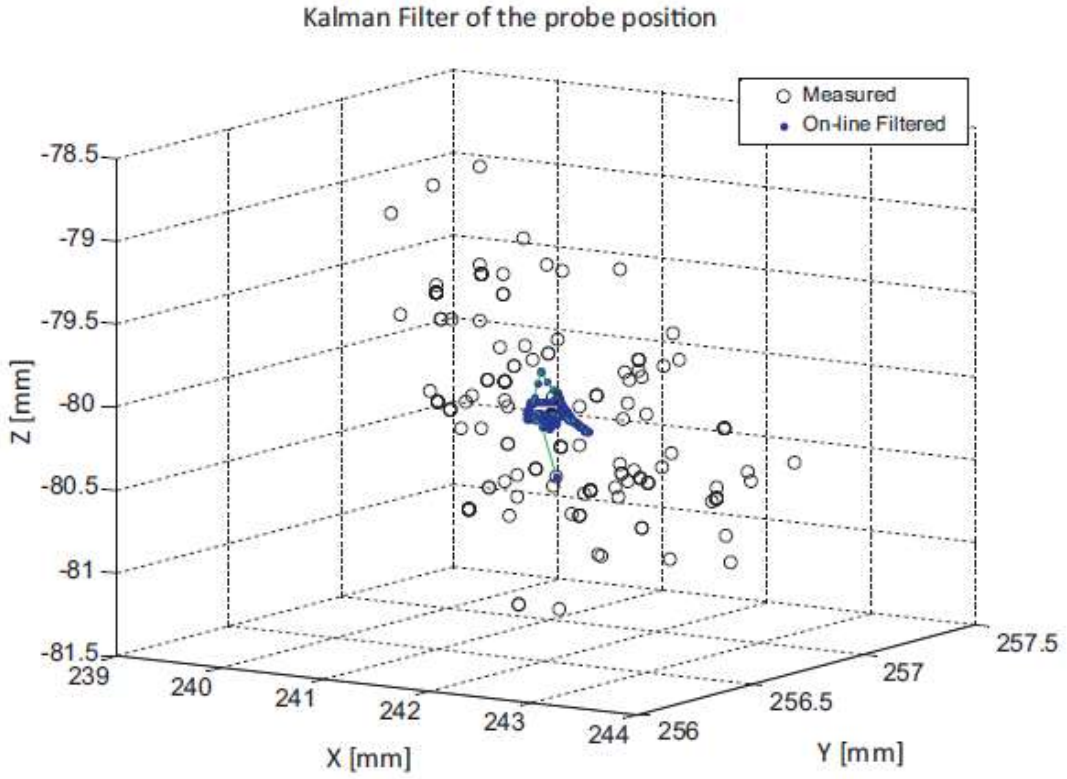

Fig. 3-6 Example of application of Kalman filter.

3.5 Artifact-based calibration algorithm

Self-calibration method of MScMS-II system has been discussed in previous section (refer to section 2.2.5). However, it is noteworthy that, some tests conducted by (Maurizio Galetto et al. 2013) based on the self-calibration method have shown that most of the volumetric error present in the system was linked to the lack of traceability system itself: the residual volumetric error was quite small, but the measurement result on a reference calibrated artifact where systematically smaller than the calibrated value.

This section introduces an artifact-based calibration algorithm (Maurizio Galetto et al. 2015), in which a calibrated artifact has been used, which carries a couple of balls separated by about 800 mm, the distance between the balls having been calibrated with micrometric accuracy. The artifact carries as well six more balls. The distances between a reference ball and the other balls has been calibrated, so that it is possible to use the calibrated artifact for the performance verification (and evaluation) of the MScMS-II in a way similar to the one proposed by the ISO 10360-2 standard for Cartesian CMM.

Generally, the problem of calibration can be considered as the problem of correctly turning the sensor outputs into the measurement results. If calibration is perfect, then no volumetric error model is required. However, because the model for calibration is usually assumes sensors are perfect, usually some residual volumetric is present, and a correction is required.

Two steps compose the mathematics that turns the cameras output into the corrected coordinates of sampled points. The first step is the so called "localization algorithm". The localization algorithm is well defined in the literature concerning photogrammetry (Thomas Luhmann et al. 2006, Marek Franaszek et al. 2011). Its complete description goes beyond the aims of the present work; here it is sufficient to remember that to apply the localization algorithm a series of parameters, summarized for every camera by the projection 3x4 real matrices $\mathbf{P}_i$, have to be defined. The application of the localization algorithm turns the camera output into the Cartesian coordinates of the point $\boldsymbol{x} = [x, y, z]^T$. An incorrect definition of these parameters leads to a distortion in this conversion, i.e. a volumetric error.

Then a definition of the camera projection matrices can be considered as a "first order error model", which can then take into account part of the volumetric error. In practice, every error which would be generated by an incorrectly calibrated but optically perfect camera is considered by this first error model (Maurizio Galetto et al. 2015). However, usually the localization algorithm does not take into account optics aberrations and other similar errors which go beyond a perfect system. To describe the volumetric error generated by these defects, a "second order error model" has been proposed by (Maurizio Galetto et al. 2015). In general, the output of the first order error model is a vector of Cartesian coordinates. Any function $\tilde{\boldsymbol{x}} = f(\boldsymbol{x})$ can be in principle considered as a possible "second order volumetric error model" (Maurizio Galetto et al. 2015), which can correct the residual volumetric error after the first order model has been correctly evaluated and the localization algorithm applied.

The choice of the correct model can be suggested by the actual kind of sensors and optics adopted, but probably it would be easier to empirically choose the model among generic (polynomial, linear, spline) models, which are easier to manage (Maurizio Galetto et al. 2015).

Kruth et al (Jean-Pierre Kruth et al. 1994) supposes that the artifact is perfectly rigid, so that the distances between couples of points are constant. The application of this concept is particularly simple in the considered case: for the MScMS-II a ball-bar, can be adopted; therefore, it should be sufficient to verify that the length of the artifact is constant in every view. The general principles for this self-calibration are then the following:

1. measure the artifact in several views;
2. define a volumetric error model which guarantees the length of the artifact is constant every view.

In fact, this is not sufficient to guarantee the traceability of the measurement, since a simple degenerate solution could satisfy this criterion, i.e. $\tilde{\boldsymbol{x}} = \mathbf{0}$. With this solution, the artifact length is perfectly constant, but this is not an acceptable solution. Therefore, Kruth (Jean-Pierre Kruth et al. 1994) introduced the need of a reference measurement performed on an artifact of known length. The original objective function introduced by Kruth was then:

$$min_{\mathrm{a}} \left[\sum_{j=1}^{m-1} (d_j(\mathbf{a}) - d_{j+1}(\mathbf{a}))^2 + \sum_{j=1}^{r} (d_j^m(\mathbf{a}) - d_j^R)^2 \right] \tag{3-14}$$

where m is the number of views, r is the number of measurement of the reference artifact, $\mathbf{a}$ is a vector of parameters on which the first and second order error model depend, $d_j(\mathbf{a})$ is the measured length of the uncalibrated artifact in the j^{th} view, $d_j^m(\mathbf{a})$ is the j^{th} measurement result of the calibrated artifact, and r is the number of measurements of the calibrated artifact. As apparent, due to the compensation of the measurement, every measured length depends on $\mathbf{a}$.

However, the MScMS-II system suffers a relevant scale error (Maurizio Galetto et al. 2013). This has suggested to switch from a self-calibration procedure to a calibration procedure. In order to avoid the need of a complete redesign of the procedure, it is sufficient to drop the first part of Eq. 3-14, to retain only the calibrated artifact related part of the optimization function. The proposed (Maurizio Galetto et al. 2015) objective function is then:

$$min_{\mathrm{a}} \left[\frac{1}{r} \sum_{j=1}^{r} (d_j^m(\mathbf{a}) - d_j^R)^2 \right] \tag{3-15}$$

This is the objective function adopted for the definition of the correct value of $\mathbf{a}$. The problem is essentially a non-linear least squares problem that can be solved by classical least squares

numerical algorithms (Donald W Marquardt 1963, Gene H Golub and Christian Reinsch 1970, Charles L Lawson and Richard J Hanson 1974, Ake Björck 1996).

In order to yield an accurate evaluation of the model defined by Eq. 3-15, two general recommendations can be suggested:

1. the whole measuring volume of MScMS-II should be covered;
2. several different positions and orientations of the artifact should be considered in order to guarantee reversal (Chris J Evans et al. 1996).

The MScMS-II system can work at a sampling rate of 50 Hz, therefore the operator just needs to move the artifact in the measurement volume at a moderate speed, so that the system is allowed to take a large number of measurements. The operator will also take care of randomly rotating the artifact while moving it, so that reversal is ensured. To cover the whole measurement volume, a calibrated artifact that consists of a series of eight infrared retroreflective spheres fixed to an aluminum bar (Fig. 3-7).

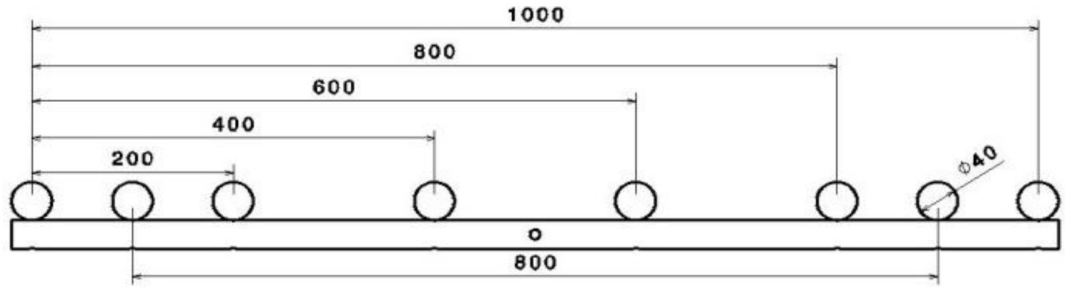

(a)

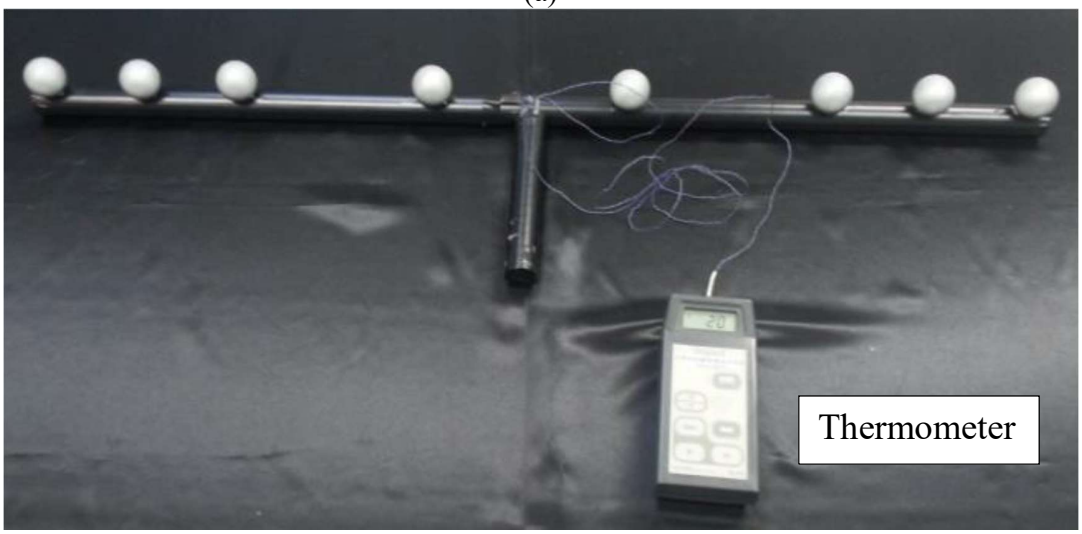

(b)

Fig. 3-7 (a) Scheme of the proposed artifact (unit: mm). (b) Manufactured artifact. (adapated from (Maurizio Galetto et al. 2015), with permission)

The artifact can be used as both calibration and verification artifact: a couple of "reference" balls, located at a nominal distance of 800 mm from each other, servers for calibration; among the remaining balls, the leftmost is considered as 0-ball. The set of 200, 400, 600, 800 and 1000 mm distances from this ball can be considered for performance evaluation/verification like in the ISO 10360-2 standard (ISO 2009).

A contact thermometer is involved in the data collection (Fig. 3-7.b), in order to measure and monitor the temperature changes during the data collection. Table 3-1 reports the calibrated lengths and uncertainties. All uncertainties are lower than 3µm, which is adequate for the expected performance of the system (around 0.1 mm).

Table 3-1 Calibration results for the manufactured artifact. (adapted from (Maurizio Galetto et al. 2015), with permission)

Nominal distance [mm]	Calibrated distance [mm]	Expanded uncertainty [µm]	Coverage factor
200	200.432	1	2
400	400.328	1.4	2
600	600.818	1.3	2
800	800.968	1.9	2
1000	1001.030	2.1	2
800 (reference)	800.852	2.8	2

An experimental campaign has been undertaken to test the effectiveness of the model (Maurizio Galetto et al. 2015). This campaign consisted in taking three series of data.

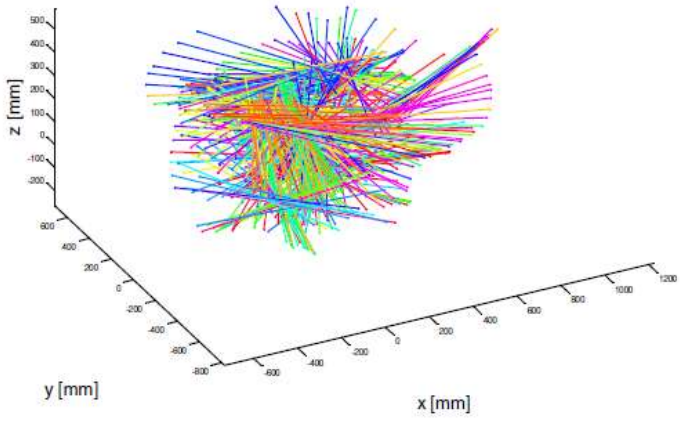

Fig. 3-8 Visualization of the artifact measurements in the first series of measurements. (adapted from (Maurizio Galetto et al. 2015), with permission)

The first dataset consists in a series of 9207 samplings of the artefact shown in Fig. 3-7.b, considering as only the "reference" couple of balls, covering a measurement volume of about 2x2x1m^3. Taking these measurements required about a couple of minutes. This "initial" data will serve to feed a non-linear least square optimization algorithm which will solve problem in Eq. 3-15. A visualization of the artifact moved through the measuring volume is shown in Fig. 3-8.

The second dataset consists of 9402 measurements of the artifact. This "check" data will serve to check that the model evaluated based on the initial data is good to compensate any measurement, and not adapted to the initial data only.

Finally, a series of about 5000 measurements has been taken for each of the five calibrated lengths given by the five couples of balls. These measurements will serve to propose an evaluation of the system performance.

In the remaining part of this section, three general purpose fitting models (i.e. polynomial model, piecewise linear model and piecewise spline model) proposed by (Maurizio Galetto et al. 2015) to define a second order volumetric error model are presented. Together with these models a "0" model will be considered, i.e. a model in which no second error correction is present but only the projection matrices parameters are adjusted.

3.5.1 Polynomial model

The polynomial model consists in a simple polynomial correction of the coordinate at which the point is measured, so the model can be written as:

$$\begin{bmatrix}\tilde{x}\\ \tilde{y}\\ \tilde{z}\end{bmatrix} = \begin{bmatrix} x + \sum_{i=0}^{g} (\beta_{ix,x} x^i + \beta_{ix,y} y^i + \beta_{ix,z} z^i) \\ y + \sum_{i=0}^{g} (\beta_{iy,x} x^i + \beta_{iy,y} y^i + \beta_{iy,z} z^i) \\ z + \sum_{i=0}^{g} (\beta_{iz,x} x^i + \beta_{iz,y} y^i + \beta_{iz,z} z^i) \end{bmatrix} \quad (3\text{-}16)$$

where the various β are optimization parameters and g is the polynomial degree (in this experience g=4). In this case, the parameter vector **a** in Eq. 3-15 is constituted by $12n_c+9g$ parameters, where n_c is the number of cameras constituting the MScMS-II.

3.5.2 Piecewise linear and spline model

In piecewise models a cubic grid of $n_p \times n_p \times n_p$ points covering the measurement volume is defined (in this experience n_p=5). For each point, a value of the volumetric correction which has to be applied at that coordinate is defined for x, y, z, so that there are $3n^3_{\mathrm{p}}$ values of the

correction. To obtain the correction value at any coordinate, the n^3_p corrections at the defined points are interpolated either linearly (piecewise linear model) or by means of a cubic spline (piecewise spline model). In this case, the parameter vector **a** in Eq. 3-15 is constituted by $12n_c+3n^3_p$ optimization parameters.

3.5.3 Results of volumetric error compensation

Table 3-2 reports the values of the average value and standard deviation of the residuals from the calibrated distance of the reference couple of balls. The column "optimization data" refers to the measurements (i.e. the first dataset) that have been fed to the optimization algorithm to evaluate the parameters. The column "check data" refers to the additional measurements which have been performed on the reference couple of balls. A high (absolute) value of the mean indicates the presence of some bias, while the standard deviation is related to the repeatability of the measurement. The row "no model" refers to the condition in which no optimization is performed, neither on the first or second order error model. The remaining four rows refer to the various error models considered.

Table 3-2 Calibration results. (adapted from (Maurizio Galetto et al. 2015), with permission)

	Optimization data		Check data	
model	mean	standard deviation	mean	standard deviation
no model	-11.08	11.1044	-4.4548	8.1370
0-model	-0.006	1.0054	-0.4130	1.6060
polynomial	0.001	1.0046	-0.4130	1.6036
piecewise linear	-0.001	0.7518	-0.3618	4.2353
piecewise spline	-0.001	0.6437	88.0815	295.0452

From the first row, it is apparent that if no error model is considered the measurement performed by MScMS-II are both biased and scarcely repeatable. Now, consider the column "optimization data": this column suggests that any model is capable of correcting the bias. In fact, all the mean values almost equal to zero. The standard deviation reduces significantly, too, indicating a repeatability improvement. However, this appearance could be explained by an "over-fitting" of the optimization data. To understand the effectiveness of the first and second order error model, one should focus on the "check data" column, which is not affected by the optimization algorithm, and then will not be affected by over-fitting. This column suggests that bias is at least reduced by an order of magnitude (from about 4 mm to about 0.4

mm). The repeatability improve as well of approximately an order of magnitude for the 0 and polynomial model. This not apply to the spline model, which gives anomalous results. In fact, the spline model seem to be the best one when applied to the optimization data, and the worst when applied to the check data. This suggest that the spline model is very prone to over-fitting, and needs an improvement in robustness. By reducing the number of nodes, it could possibly avoid over-fitting, but this could also neglect the expected advantages of the spline model. In summary, one can conclude that the best performance is yielded when either 0 or the polynomial model is applied (Maurizio Galetto et al. 2015).

Fig. 3-9 reports the performance obtained from the third dataset, which refers to the measurement of five couples of balls placed at a reciprocal nominal distance equal to 200, 400, 600, 800, and 1000 mm respectively. Fig. 3-9 plots the residuals from the calibrated lengths for the various proposed models. Again, the 0 and polynomial models seem to be the best models, significantly improving the results available when no correction is applied, while the spline models yield inconsistent results. Fig. 3-9 proposes an evaluation of the MPE (Maximum Permissible Error) for the various models, as suggested in the ISO 10360-2 standard. The red lines graphically represent this performance in Fig. 3-9. The green lines indicate the performance when no correction is applied. Please note that this performance evaluation does not neglect the probing error: in fact, the camera adopted does not give as output a cloud of points on the surface of the balls, but only the centers of the balls directly, since the balls mounted on the long bar are the reconstructed targets themselves. Therefore, this performance correctly estimates the performance of the system considered as tracking system. However, the portable measuring probe has not been used in this performance evaluation, thus its influence is neglected.

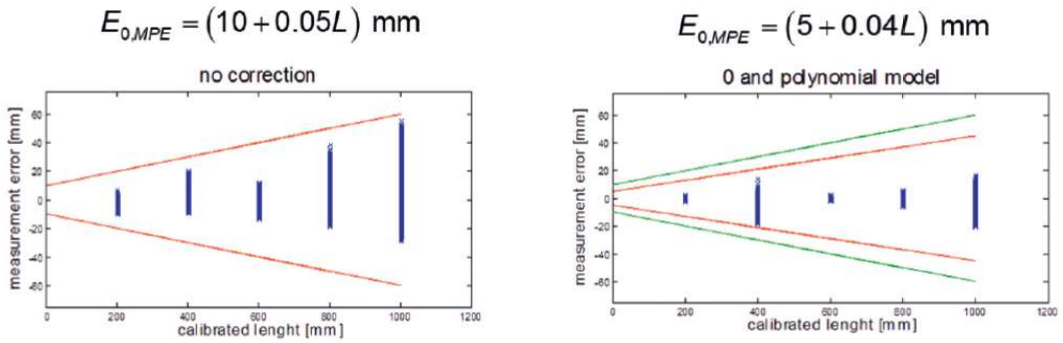

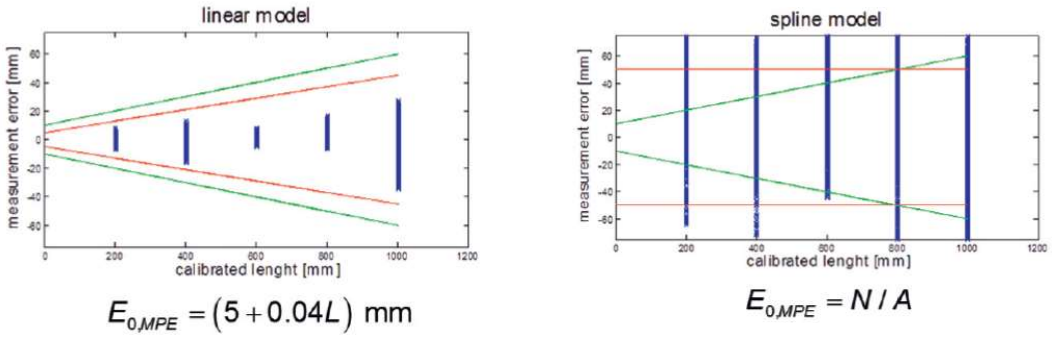

Fig. 3-9 Performance of the MScMS-II based on measurement of a calibrated artifact. (adapted from (Maurizio Galetto et al. 2015), with permission)

3.6 Summary of error correction methods

This chapter presents a series of studies on error correction methods for improving the performance of MScMS-II. In general, the performance of MScMS-II is influence by both random errors, which cannot be corrected, and systematic errors, which are due to imperfect hardware and/or imperfect determination of the system parameters and to other not corrected aberrations, and can be compensated if known. The sources of systematic errors considered in this study include (i) lens distortion, (ii) physical size of the probe tip, (iii) the kinematic of the probe during measuring process, and (iv) imperfect determination of the calibration parameters, which are essentially relevant to optical-based systems that are based on triangulation principle and do measurement using a contact probe. By developing error correction model for each error source, the performance of system is improved by up to an order of magnitude with respect to that before error correction (Maurizio Galetto and Luca Mastrogiacomo 2013, Maurizio Galetto et al. 2015).

Although some random and systematic errors could be reduced to some extent if more advanced and accurate cameras are introduced to the system (e.g., lens distortion could be irrelevant with perfectly manufactured but costly lenses), the research in error compensation indeed improves the system performance given a limited budget of hardware, and furthermore, it opens several research scenarios for the improvement of the system, for example, the study of the kinematics of the probe led to the introduction of the Kalman filter to filter the noise that the instrument introduces to the static measurement. The natural extension of the model to the cinematic case has still to be considered and analyzed.

4. Diagnostic technique for monitoring system stability

4.1 Introduction

This chapter presents a diagnostic technique for monitoring system stability of multi-camera system, which can be easily integrated into calibration software without the need of additional procedures or artifacts. The proposed technique is based on multivariate control charts and has been verified on a custom-made assembled system (implementation of the system is to be provided in chapter 5).

As previously described, the MScMS-II is a multi-camera system designed for LSDM (Large-Scale Dimensional Metrology) applications, whose metrological performance is critically related to the correctness of estimation of system parameters, through calibration techniques. Calibration produces the values for external and internal parameter given the operation constraints (Edward M Mikhail et al. 2001, Thomas Luhmann et al. 2006, Maurizio Galetto et al. 2010a). External parameters describe the spatial configuration of the system, i.e. position and orientation of the cameras in the measurement space. These parameters change whenever cameras are moved. On the other hand, internal parameters describe the technical characteristics of the cameras. These parameters, change when camera-specific elements are altered, such as lenses or settings, or if drift/damage occurs. Several different procedures for calibration are described in literature, e.g. based on the use of calibrated artifacts, implementation of specific procedures, or a combination of both (C BROWN Duane 1971, Roger Y Tsai 1987, Zhengyou Zhang 2000, Edward M Mikhail et al. 2001, T. Svoboda et al. 2005, Thomas Luhmann et al. 2006, Song Zhang and Peisen S Huang 2006, J.Y Bouguet 2015).

For those situations that require a continuous and/or long-term monitoring of some dimensional process, such as production lines, calibration parameters are updated regularly in order to ensure optimal performance. In these cases, current approaches incorporate calibration into the measurement process with no additional hardware effort. These procedures may guarantee reliable and accurate results, limiting the regular use of external artifacts. See, for example, commercial photogrammetric systems Quality Gate by Mapvision or TubeInspect by Aicon (Aicon , Mapvision).

The correctness of calibration may be checked using reference artifacts, a proven, reliable approach, the implementation of which may, however, be difficult, expensive and time consuming (Edward M Mikhail et al. 2001, Thomas Luhmann et al. 2006). An alternative approach may be based on the monitoring of internal parameters after each calibration, thereby relying on control of stability (IEC BIPM et al. 2008) of camera parameters in order to check correctness of calibration.

The use of multivariate control charts for monitoring internal parameters is proposed in this part of dissertation. In general, multivariate control charts are used whenever simultaneous

control of two or more quality characteristics is required (Harold Hotelling 1947, Douglas C Montgomery 2007). The proposed technique applies multivariate control charts as diagnostic tools for evaluating the stability of internal parameters after each calibration; calibration results are directly used for the diagnosis.

The remaining part of this chapter is organized as follows:

- section 4.2 describes the mathematical model of a custom-made multi-camera system, which characterizes the system into a series of parameters that describes the technical characteristics and spatial configuration of the distributed cameras; and defines the relevant parameters that attributes to the system stability;
- section 4.3 introduces two well-known calibration techniques proposed in the scientific literature by (T. Svoboda et al. 2005) and (J.Y Bouguet 2015) respectively, which are adapted to the custom-made multi-camera system;
- section 4.4 presents the diagnostic technique based on multivariate control charts, i.e. the well-known Hotelling T^2 and Generalized Variance, for monitoring the stability of camera parameters;
- section 4.5 provides the results of an experimental campaign to verify the effectiveness of proposed diagnostic approach and presents a structured comparison between two calibration techniques based on the results; lastly, this chapter is summarized with the innovative aspects of the diagnostic tool.

4.2 Mathematical model of camera system

The metrology model of the camera system, which links the 3 dimensional coordinates (x_j, y_j, z_j) to the 2 dimensional coordinates $(u_{i,j}, v_{i,j})$ in image plane, is shown as below:

$$\begin{bmatrix} u_{i,j} \\ v_{i,j} \\ 1 \end{bmatrix} = \mu_i \mathbf{K}_i \mathbf{W}_i \begin{bmatrix} x_j \\ y_j \\ z_j \\ 1 \end{bmatrix} = \mathbf{P}_i \begin{bmatrix} x_j \\ y_j \\ z_j \\ 1 \end{bmatrix} \tag{4-1}$$

where $\mu_i \in \mathbb{R}^+$ is a non-zero scale factor, $\mathbf{K}_i \in \mathbb{R}^{3,4}$ is the matrix of internal parameters (i.e. the two coordinates of the image center u_{0_i} and v_{0_i}, and the camera-related components u_{f_i} and v_{f_i} of the focal length l_{f_i} in the camera view plane, expressed in pixels), defined as:

$$\mathbf{K}_i = \begin{bmatrix} u_{f_i} & 0 & u_{0_i} & 0 \\ 0 & v_{f_i} & v_{0_i} & 0 \\ 0 & 0 & 1 & 0 \end{bmatrix} \tag{4-2}$$

and $\mathbf{W}_i \in \mathbb{R}^{4,4}$ is the matrix of external parameters (i.e. the camera projection center coordinates x_{c_i}, y_{c_i} and z_{c_i}, and the camera orientation angles ω_i, ϕ_i, and κ_i in the world coordinate reference frame F_{WCS}, see Fig. 2-15), defined as:

$$\mathbf{W}_i = \begin{bmatrix} & & & -x'_{C_i} \\ & \mathbf{R}_i & & -y'_{C_i} \\ & & & -z'_{C_i} \\ 0 & 0 & 0 & 1 \end{bmatrix} \tag{4-3}$$

being x'_{c_i}, y'_{c_i} and z'_{c_i} the coordinates of the projection center $C_i \equiv \begin{pmatrix} x_{C_i} & y_{C_i} & z_{C_i} \end{pmatrix}$ in the local camera reference frame F_{CCS}, and $\mathbf{R}_i \in \mathbb{R}^{3,3}$ the rotation matrix, which relates the world coordinate reference frame F_{WCS} and the local camera reference frame F_{CCS}, as shown in Fig. 4-1. The so obtained matrix $\mathbf{P}_i \in \mathbb{R}^{3,4}$ is called camera projection matrix.

The ideal model descried in Eq. 4-1 provides only an approximation because imaging error are liable to substantially affect the accuracy of localization of optical markers. Corrections are applied to the image coordinates in order to consider lens distortion errors. According to scientific literature, imaging errors are mainly related to radial, tangential and skewness distortion (Edward M Mikhail et al. 2001, Thomas Luhmann et al. 2006), These error components are usually evaluated using polynomial models, whose coefficients are denoted as distortion coefficients. The total lens distortion correction, as introduced in the collinearity equations, can be expressed as:

$$\begin{bmatrix} \tilde{u}_{i,j} \\ \tilde{v}_{i,j} \\ 1 \end{bmatrix} = \begin{bmatrix} 1 & 0 & \delta u_{R;i,j} + \delta u_{T;i,j} + \delta u_{S;i,j} \\ 0 & 1 & \delta v_{R;i,j} + \delta v_{T;i,j} \\ 0 & 0 & 1 \end{bmatrix} \begin{bmatrix} u_{i,j} \\ v_{i,j} \\ 1 \end{bmatrix} \tag{4-4}$$

where $\delta u_{R;i,j}$ and $\delta v_{R;i,j}$ represent the radial distortion:

$$\begin{aligned} \delta u_{R;i,j} &= \left[k_{C1,i} \cdot \left(u_{i,j}^2 + v_{i,j}^2 \right) + k_{C2,i} \cdot \left(u_{i,j}^2 + v_{i,j}^2 \right)^2 + k_{C5,i} \cdot \left(u_{i,j}^2 + v_{i,j}^2 \right)^3 \right] u_{i,j} \\ \delta v_{R;i,j} &= \left[k_{C1,i} \cdot \left(u_{i,j}^2 + v_{i,j}^2 \right) + k_{C2,i} \cdot \left(u_{i,j}^2 + v_{i,j}^2 \right)^2 + k_{C5,i} \cdot \left(u_{i,j}^2 + v_{i,j}^2 \right)^3 \right] v_{i,j} \end{aligned} \tag{4-5}$$

$\delta u_{T;i,j}$ and $\delta v_{T;i,j}$ are the components related to the tangential distortion:

$$\begin{aligned} \delta u_{T;i,j} &= 2 \cdot k_{C3,i} \cdot u_{i,j} \cdot v_{i,j} + k_{C4,i} \cdot \left(3 \cdot u_{i,j}^2 + v_{i,j}^2 \right) \\ \delta v_{T;i,j} &= 2 \cdot k_{C4,i} \cdot u_{i,j} \cdot v_{i,j} + k_{C3,i} \cdot \left(u_{i,j}^2 + 3 \cdot v_{i,j}^2 \right) \end{aligned} \tag{4-6}$$

and $\delta u_{S;i,j}$ is related to the skewness distortion:

$$\delta u_{S;i,j} = \alpha_i \cdot v_{i,j} \tag{4-7}$$

Besides those parameters classified as internal parameters (u_{0_i}, v_{0_i}, u_{f_i}, v_{f_i} and α_i) and external ones (x_{c_i}, y_{c_i}, z_{c_i}, ω_i, ϕ_i and κ_i), lens distortion (radial, tangential and skew distortion effect) are the factors that influence the accuracy of localizing the points of interest. The aim of calibration is to estimate these coefficients as precise as possible, in order to reduce the overall uncertainty in point localization.

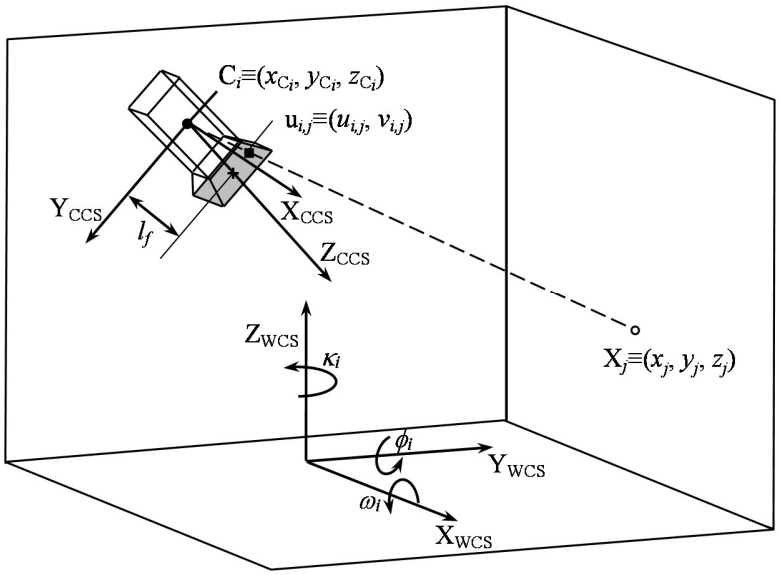

Fig. 4-1 Setup of a generic camera-based localization problem in the 3D space. (adapted from (Fiorenzo Franceschini et al. 2011), with permission)

4.3 Calibration techniques

The performance of distributed metrology systems is strongly related to several factors that can affect the accuracy of the system adversely, such as the number of network devices, the set-up parameters, and the relative position in the working volume of the points to be measured (Fiorenzo Franceschini et al. 2011). Optical systems, relying on the use of multiple cameras and photogrammetric techniques, require a preliminary calibration procedure to determine some essential parameters, such as camera positions and orientations, focal length, distortion parameters, etc. (Ou Bai et al. 2014). This section describes the calibration strategies applied to the prototype system.

Many different calibration techniques have been presented in the literature (Edward M Mikhail et al. 2001, T. Svoboda et al. 2005, Thomas Luhmann et al. 2006, Song Zhang and Peisen S Huang 2006, J.Y Bouguet 2015), two calibration approaches are discussed in (Ou Bai et al. 2014) due to their broad usability and relevance in the literature.

4.3.1 Self-calibration based on a randomly moved marker

Svoboda et al. (T. Svoboda et al. 2005) proposed an approach able to estimate simultaneously internal and external parameters of cameras without exploiting special artifacts but only using a marker (i.e. a 40 mm diameter reflective sphere) randomly moved in the field of view of system cameras (see Fig. 4-2).

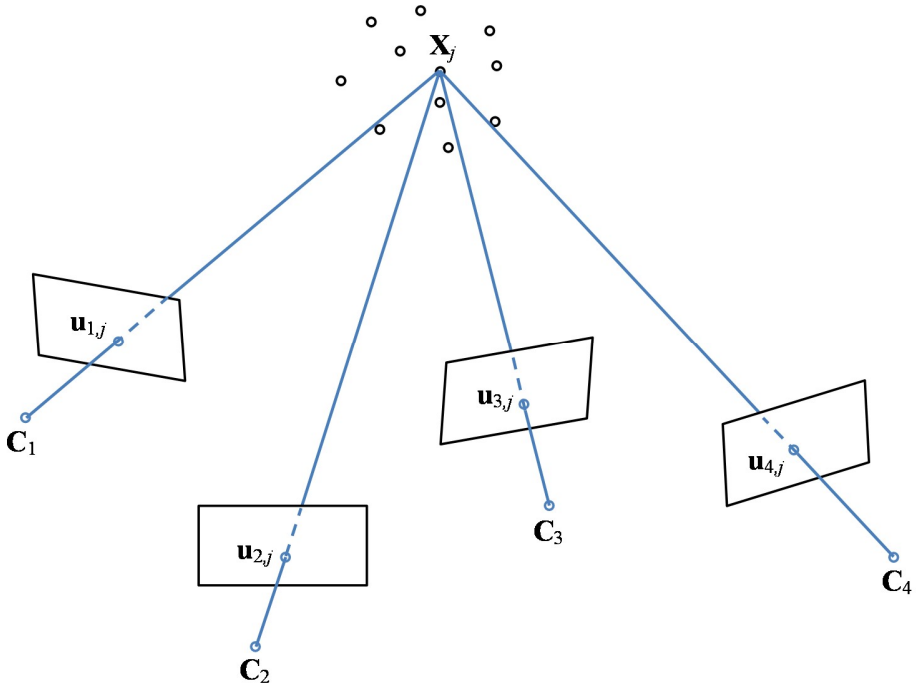

Fig. 4-2 Scheme of self-calibration of multi-camera system according to the algorithm proposed by (T. Svoboda et al. 2005).

The goal of the calibration is to estimate for each camera the scale parameter μ_i, the projection matrix $\mathbf{P}_i$ and the correction parameters.

Given n points (marker positions) and m cameras, this can be obtained starting from the following expression:

$$\mathbf{Q} = \begin{bmatrix} \mu_1 \begin{bmatrix} u_{1,1} \\ v_{1,1} \\ 1 \end{bmatrix} & \cdots & \mu_1 \begin{bmatrix} u_{1,n} \\ v_{1,n} \\ 1 \end{bmatrix} \\ \vdots & \vdots & \vdots \\ \mu_m \begin{bmatrix} u_{m,1} \\ v_{m,1} \\ 1 \end{bmatrix} & \cdots & \mu_m \begin{bmatrix} u_{m,n} \\ v_{m,n} \\ 1 \end{bmatrix} \end{bmatrix} = \begin{bmatrix} \mathbf{P}_1 \\ \vdots \\ \mathbf{P}_m \end{bmatrix} \begin{bmatrix} \mathbf{X}_1 & \cdots & \mathbf{X}_n \end{bmatrix} \tag{4-8}$$

where $\mathbf{X}_j = \begin{bmatrix} x_j & y_j & z_j & 1 \end{bmatrix}^T$ (with $j = 1 \ldots n$).

Eq. 4-8 may be rewritten in the following compact form:

$$\mathbf{Q} = \mathbf{PX} \tag{4-9}$$

where $\boldsymbol{P} = [\boldsymbol{P_1} \ldots \boldsymbol{P_m}]$ and $\boldsymbol{X} = [\boldsymbol{X_1} \ldots \boldsymbol{X_n}]$.

Q is called the scaled measurement matrix, **P** and **X** are referred as the projective motion and the projective shape respectively. If enough noiseless points $\mathbf{u}_{i,j} = \begin{bmatrix} u_{i,j} & v_{i,j} & 1 \end{bmatrix}^T$ (with $i = 1 \ldots m$ and $j = 1 \ldots n$) are collected and all scale parameters μ_i are known, then **Q** has rank 4 and can be factorized into **P** and **X**. It should be noted that the only input is the collected set of points $\mathbf{u}_{i,j} = \begin{bmatrix} u_{i,j} & v_{i,j} & 1 \end{bmatrix}^T$.

However, scale parameters μ_i are not known in advance, moreover, some of the points $\mathbf{u}_{i,j} = \begin{bmatrix} u_{i,j} & v_{i,j} & 1 \end{bmatrix}^T$ may be missing because of shadowing or simply misdetections. In order to compute the scale parameters μ_i the missing points are filled in by applying rank-4 constraints (Amnon Shashua and Shai Avidan 1996).

The factorization of Eq. 4-9 recovers the motion and the shape up to a 4x4 projective transformation **H**:

$$\boldsymbol{Q = PX = PHH^{-1}X = \widehat{P}\widehat{X}} \tag{4-10}$$

where $\hat{\mathbf{P}} = \mathbf{PH}$ and $\hat{\mathbf{X}} = \mathbf{H}^{-1}\mathbf{X}$. Any non-singular 4x4 matrix may be inserted between **P** and **X** to get another compatible motion and shape pair ($\boldsymbol{\widehat{P}, \widehat{X}}$). The self-calibration process computes such a matrix **H** so that $\boldsymbol{\widehat{P}}$ and $\boldsymbol{\widehat{X}}$ become Euclidean, in the scientific literature this

process is often called Euclidean stratification (Richard Hartley and Andrew Zisserman 2004). The task of finding the appropriate **H** can be achieved by imposing specific geometrical constraints. The most general constraint is the assumption that rows and columns of camera chips are orthogonal. Alternatively, it can be assumed that some internal parameters of the cameras are the same, which is more useful for a monocular camera sequence.

The working procedure is based on two steps:

(i) reconstruction of the calibration points by using the linear parameters;

(ii) feed of these 3D-2D correspondences into a standard method for estimation of the nonlinear distortion and repeat the self-calibration with the undistorted points.

This estimate-and-refine cycle is repeated until it reaches a required precision. This coupled iterative approach yields typically an average re-projection error less than 1/4 pixel (T. Svoboda et al. 2005).

4.3.2 Calibration with a chessboard

Bouguet (J.Y Bouguet 2015) proposed another approach which involves the use of a calibrated reference artifact, i.e. a chessboard with a known geometry (see Fig. 4-3), which usually consists of 7x7 square blocks in black and white surrounded by a peripheral reference zone (this dimension is scalable if needed, i.e. 8x8, 9x9, etc.).

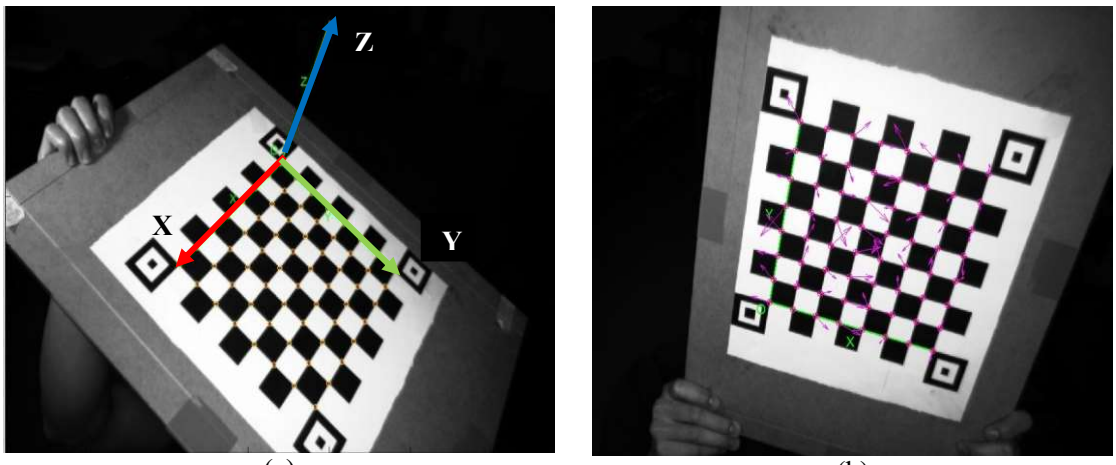

(a) (b)

Fig. 4-3 (a) Corners of chessboard squares (corner points) and reference coordinate system (X, Y and Z lines); (b) re-projection errors (line with arrows) in one image.

The quality and the planarity of the chessboard have non-negligible impact on the result of the calibration, so the geometry of the chessboard has to be accurately calibrated *a priori*.

The method consider each camera taken individually. For a given camera *i*, after having defined a reference coordinate system on the chessboard (see the coordinate system marked

in Fig. 4-3.a), the 3D coordinates $\mathbf{X}_j = \begin{bmatrix} x_j & y_j & z_j & 1 \end{bmatrix}^T$ (with j=1,…,n, where n=8x8=64 is the total number of corners) of each corner of the squares are defined through a specific calibration procedure and recorded in matrix $\mathbf{X} = [\mathbf{X}_1 \quad \cdots \quad \mathbf{X}_n]$. Then, the toolbox developed by Bouguet extracts the 2D coordinates $\mathbf{u}_{i,j} = \begin{bmatrix} u_{i,j} & v_{i,j} & 1 \end{bmatrix}^T$ of each square corner from the 2D image in the plane of view of the camera (see points in Fig. 4-3.a) and records them in matrix $\mathbf{U}_i = \begin{bmatrix} \mathbf{u}_{i,1} & \cdots & \mathbf{u}_{i,n} \end{bmatrix}$ (J.Y Bouguet 2015). Given the corresponding 2D and 3D points ($\mathbf{U}_i$, $\mathbf{X}$), the main calibration procedure is divided into two phases: initialization and non-linear optimization.

In the initialization phase, the approach neglects distortion effect and makes a preliminary estimate of internal parameters, then uses the obtained values to evaluate the external parameters and refine the internal ones.

In the non-linear optimization phase, the approach applies an iterative algorithm (Levenberg-Marquardt algorithm (Richard Hartley and Andrew Zisserman 2004, J.Y Bouguet 2015) in order to obtain a refined estimate of $\mathbf{P}_i$ and related correction parameters by minimizing $\left|\tilde{\mathbf{U}}_i - \mathbf{P}_i\mathbf{X}\right|^2$, i.e. the overall re-projection error of image corners (where $\tilde{\mathbf{U}}_i$ is the matrix of corrected 2D corners' coordinates, see Eq. 4-4), (see Fig. 4-3.b).

This operation is implemented for a set of several images taken with different positions and orientations of the chessboard. By separating the calibration procedure into two phases, a separated estimation of intrinsic/extrinsic parameters and distortion corrections can be performed.

Since the chessboard is separately moved in front of each camera in order to obtain an adequate number of images to cover as much as possible its field of view, the calibration results are independent from camera to camera.

Comparing this method to Svoboda's approach, it is shown that it needs fewer sample images since each image contains more geometric information (i.e. the total number of square corners). Furthermore, since the chessboard is calibrated before use, this approach does not entail alignment procedure after calibration.

4.4 Multivariate control charts

Monitoring internal and correction camera parameters involves dealing with several variables. Univariate control charts might be drawn up for each single variable (Douglas C Montgomery 2007), however with the drawback of misleading results should variables turn out to be correlated. Therefore multivariate methods are preferable.

Univariate control of mean and dispersion is usually dealt with X-bar and S control chart respectively (Douglas C Montgomery 2007), whose multivariate extensions are the well-known Hotelling T^2 (Harold Hotelling 1947) and the Generalized Variance control charts (Joe H Sullivan and William H Woodall 1996). However, monitoring of internal and correction camera parameters refers to the case of individual observations, one value only for each parameter being obtained at each calibration. Therefore, specific values of the control limits should be considered for both the charts.

Use of control charts covers typically two phases (Douglas C Montgomery 2007), namely Phase I, in which charts are used to test whether the process was in control when the first subgroups were drawn, and Phase II, in which charts are used to test whether the process stays in control when subsequent subgroups are drawn. In case of multivariate charts, a different form of control limits may be selected for each phase, because different distributions may be involved (William H Woodall et al. 2000).

The Hotelling T^2 statistic is a distance which accounts for the covariance structure of a multivariate normal distribution (Harold Hotelling 1947). It represents the multivariate counterpart of the Student's-*t* statistic. The formula for computing the T^2 distance, in case of individual observations, is (Harold Hotelling 1947):

$$T_i^2 = \left(\mathbf{V}_i - \bar{\mathbf{V}}\right)^T \mathbf{S}^{-1} \left(\mathbf{V}_i - \bar{\mathbf{V}}\right) \qquad i = 1,...,k \tag{4-11}$$

where k is the number of samples used for chart construction in Phase I, $\boldsymbol{V}_i$ is the vector of observations (namely, $\mathbf{V}_i = \begin{bmatrix} u_{0_i} & v_{0_i} & u_{f_i} & v_{f_i} & k_{C1,i} & k_{C2,i} & k_{C3,i} \end{bmatrix}^T$ and k=30, in the present case), $\bar{\mathbf{V}} = \frac{1}{k} \cdot \sum_{i=1}^{k} \mathbf{V}_i$ is the vector of the corresponding mean values and $\mathbf{S}$ is the Sullivan and Woodall's special covariance matrix (William H Woodall et al. 2000):

$$\mathbf{S} = \frac{1}{2 \cdot (k-1)} \mathbf{E}^T \mathbf{E} \tag{4-12}$$

where $\mathbf{E} = \begin{bmatrix} \mathbf{e}_1^T & \mathbf{e}_2^T & \dots & \mathbf{e}_{k-1}^T \end{bmatrix}^T$, and $\mathbf{e}_i$ are the differences between successive observations:

$$\mathbf{e}_i = \mathbf{V}_{i+1} - \mathbf{V}_i \qquad i = 1,...,k-1 \tag{4-13}$$

In general, the higher the T^2 value, the more distant is the observation from the mean. In Phase I, the Hotelling T^2 statistics may be approximated using a Beta distribution with parameters $\frac{p}{2}$ and $\frac{f-p-1}{2}$ (FW Scholz and TJ Tosch 1994):

$$T^2 \sim \frac{(k-1)^2}{k} \cdot Beta\left(\frac{p}{2}, \frac{f-p-1}{2}\right) \tag{4-14}$$

with

$$f = \frac{2 \cdot (k-1)^2}{3 \cdot k - 4} \tag{4-15}$$

where p is the number of process variables (namely, in the present case, p=7 is the number of estimated internal and correction parameters). Therefore, the lower and upper control limits (*LCL* and *UCL*) are the values of T^2 statistics in Eq. 4-14 corresponding to a cumulative probability of 0.135% and 99.865%; however, *LCL* is typically set to zero since any shift in the mean determines an increase in T^2.

In Phase II, the Hotelling T^2 statistic may be approximated by a Fisher distribution with p and k-p degrees of freedom (Nola D Tracy 1992):

$$T^2 \sim \frac{p \cdot (k+1) \cdot (k-1)}{k^2 - k \cdot p} \cdot F(p, k-p) \tag{4-16}$$

Therefore, *UCL* is now the value of T^2 statistic in Eq. 4-16 corresponding to a cumulative probability of 99.865% and *LCL* is set again to zero.

Referring to the chart for sample dispersion, in general, when data are collected in subsequent samples, the Generalized Variance statistic is $|\mathbf{S}|$, i.e. the determinant of the sample covariance matrix (Douglas C Montgomery 2007). In case of individual observations, all the conventional formulas for the Generalized Variance chart do not work. Therefore, it is proposed an *ad-hoc* procedure. All values are standardized by subtracting the relevant column mean and then dividing by the square root of the relevant variance taken from the Sullivan and Woodall's covariance matrix (see Eq. 4-12) (Joe H Sullivan and William H Woodall 1996):

$$V_i^*(j) = \frac{V_i(j) - \bar{V}_i(j)}{\sqrt{S_{j,j}}} \qquad i = 1,\ldots,k, \quad j = 1,\ldots,p \tag{4-17}$$

where $V_i(j)$ and $\bar{V}_i(j)$ are the j-th elements respectively of $\mathbf{V}_i$ and $\bar{\mathbf{V}}_i$ vectors. Once obtained the standardized values, a traditional S chart is adopted in which each subgroup

corresponds to the components of each $\mathbf{V}_i^*$ vector. Therefore, the values reported on the Generalized Variance chart, in case of individual observations, correspond to the standard deviations of the components of vectors $\mathbf{V}_i^*$ (Cynthia A Lowry and Douglas C Montgomery 1995):

$$S_i^* = \sqrt{\frac{\sum_{j=1}^{p}\left(V_i^*(j) - \bar{V}_i^*\right)^2}{p-1}} \qquad i = 1,\ldots,k \tag{4-18}$$

where $\bar{V}_i^* = \frac{\sum_{j=1}^{p} V_i^*(j)}{p}$ is the mean of the p components of i-th vector. Then, the control limits are:

$$\begin{aligned} LCL &= B_3 \cdot \bar{S}^* \\ UCL &= B_4 \cdot \bar{S}^* \end{aligned} \tag{4-19}$$

Where $\bar{S}^* = \frac{\sum_{i=1}^{k} S_i^*}{k}$ is the average over the k observations of the standard deviations of each vector $\mathbf{V}_i^*$, B_3 and B_4 are two standard parameters tabulated for various sample sizes on specific handbooks for SPC (Statistical Process Control) (Harold Hotelling 1947). A central line corresponding to $\bar{S}^*$ is typically shown in the chart. For the Generalized Variance charts, the calculation of control limits in Phase I and Phase II is the same.

In the approach described in this paper Phase I is considered in order to compare the regularity and stability of calibration parameters obtained using the two different calibration procedures. According to that, control limits are found using the method described above.

4.5 Results analysis

A series of k=30 calibrations have been implemented on the 3-camera prototype system using both the procedures under unchanged conditions. Owing to camera characteristics, in the two calibration procedures, parameters α_i , $k_{C4,i}$ and $k_{C5,i}$ were found to be non-significant. Therefore, for each of the three cameras, $p = 7$ parameters only, 4 internal (u_{0_i} , v_{0_i} , u_{f_i} and v_{f_i}) and 3 corrections ($k_{C1,i}$, $k_{C2,i}$ and $k_{C3,i}$), have been monitored.

Hotelling T^2 and the Generalized Variance control charts were applied to monitor these parameters. Obtained results are reported in Figs. 4-4 to 4-9 for the 3 cameras respectively. Svoboda's and Bouguet's methods have been evaluated by comparing the different profiles appearing in the plotted charts. Considering that, during the experiment, technical parameters of the cameras have been unchanged, it can be observed that generally the two methods present similar performance, however Bouguet's approach performs better in both T^2 and Generalized Variance control chart. In fact it shows major stability with all the three cameras: this is specially shown by the lower number of out-of-control points in both charts and by the lower dispersion of chart points. Taking for example Figs. 4-4.a and 4-4.b, 6 out-of-control points occur for the Svoboda's approach against 2 for Bouguet's one. Furthermore, apart from Figs. 4-5.b and 4-9.b, which show an apparent trend, all the other charts referred to the single marker approach reveal a wider dispersion of points. A qualitative comparison two calibration methods are listed in table 4-1:

Table 4-1 Main difference between the two analyzed calibration approaches.

	Svoboda	**Bouguet**
No. of cameras used	3 or more	1
Interaction between cameras	Yes	No
Use of external illuminator	Yes*	No
Tolerance to shadow	Yes	No

*Note: for Svoboda's method, light is needed if the marker is retro-reflective, not needed if it is an active marker; for Bouguet's one, reflection caused by strong light may blur the border between white and black squares, which leads to inaccuracy.

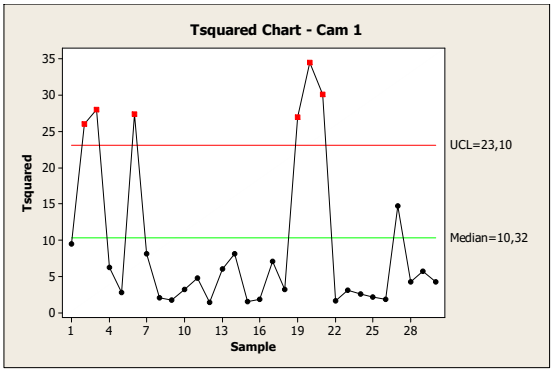

(a)

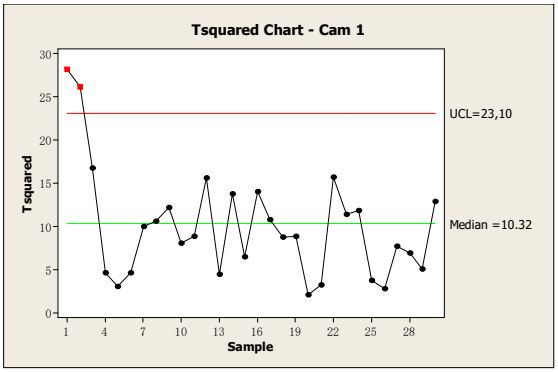

(b)

Fig. 4-4 Hotelling T^2 charts for parameters of camera 1: (a) approach using single marker; (b) approach using chessboard.

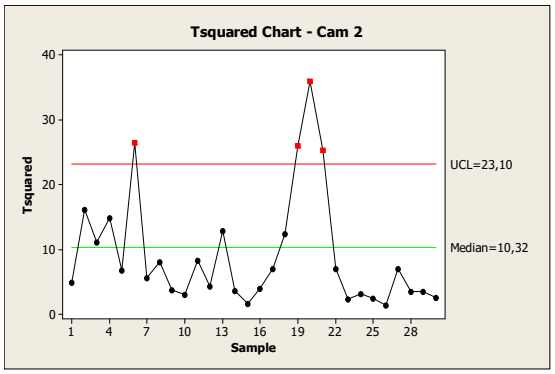

(a)

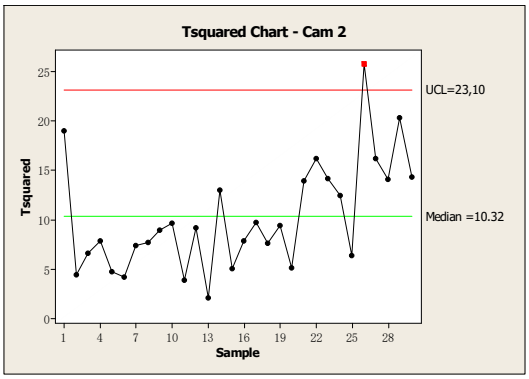

(b)

Fig. 4-5 Hotelling T^2 charts for parameters of camera 2: (a) approach using single marker; (b) approach using chessboard.

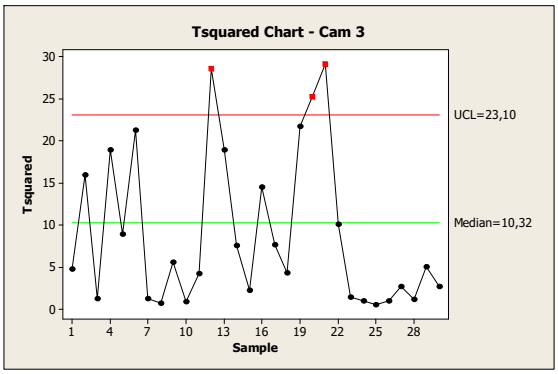

(a)

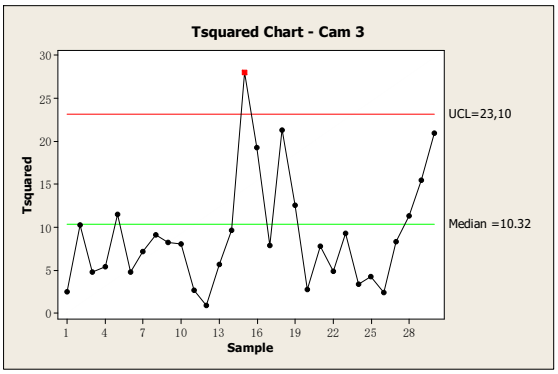

(b)

Fig. 4-6 Hotelling T^2 charts for parameters of camera 3: (a) approach using single marker; (b) approach using chessboard.

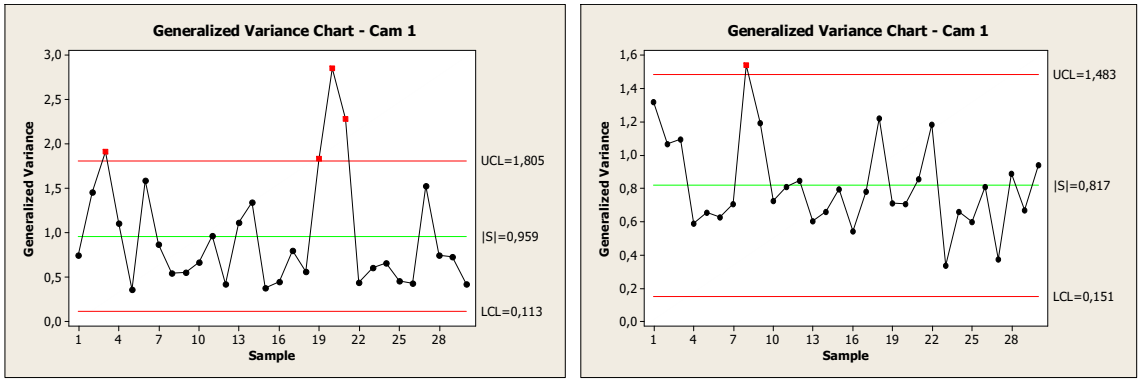

(a) (b)

Fig. 4-7 Generalized Variance charts for parameters of camera 1: (a) approach using single marker; (b) approach using chessboard.

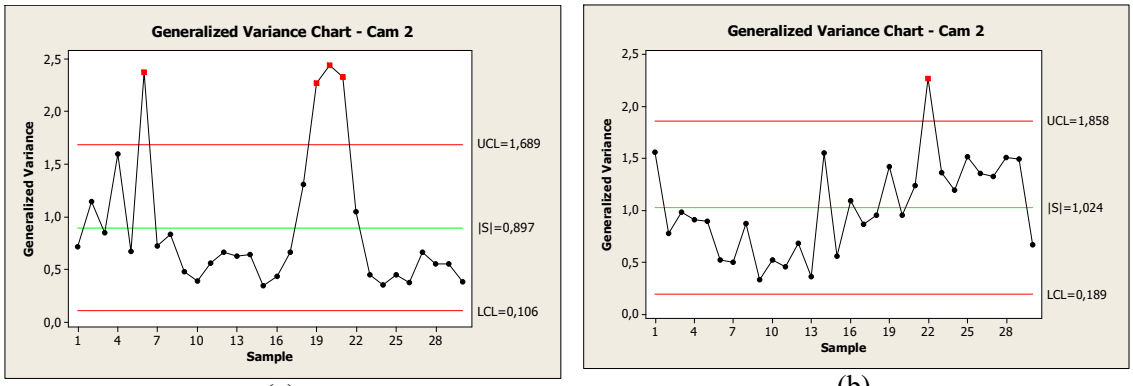

(a) (b)

Fig. 4-8 Generalized Variance charts for parameters of camera 2: (a) approach using single marker; (b) approach using chessboard.

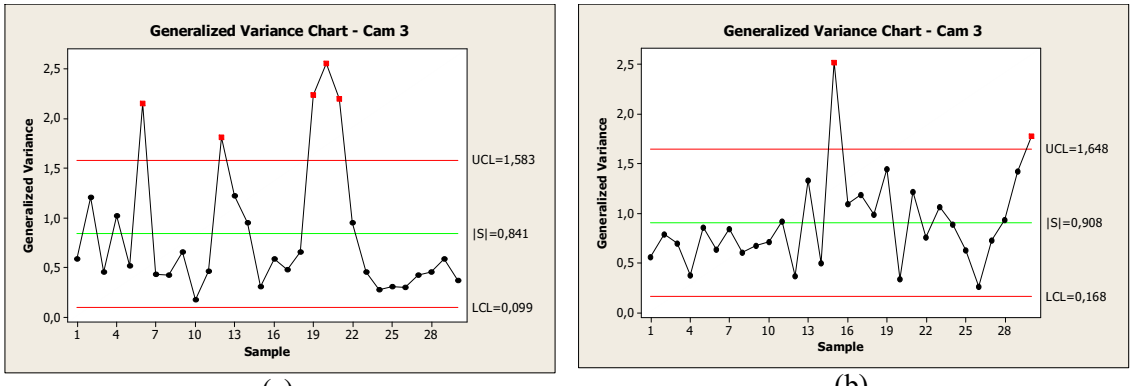

(a) (b)

Fig. 4-9 Generalized Variance charts for parameters of camera 3: (a) approach using single marker; (b) approach using chessboard.

Concerning the two analyzed procedures, Bouguet's approach present a better stability in both and Generalized Variance control chart; since Svoboda's method needs a joint use of at least three cameras, the result is somehow liable to the relative position between each pair of cameras, while Bouguet's one works independently for each camera.

On the other hand, operatively, Svoboda's approach is much easier to execute than the other one. It is only required to move randomly a spherical marker (usually with a diameter ranging from 10 to 40 mm) inside the measurement volume, then all the internal and external parameters are estimated simultaneously for all the cameras; while the Bouguet's approach needs a separate calibration upon internal and external parameters for each camera using a chessboard which is often less easy to localize due to light reflections and shadows.

A hybrid strategy of calibration, merging the advantages of the two methods, is going to be proposed in the future work in order to obtain a faster and more accurate approach, as well as integrating the control chart tool for stability control during subsequent calibrations.

5. Development of a 3-camera system prototype

As is mentioned in section 2.2.7, hardware characteristics (e.g. sensor resolution and sensitivity), camera synchronization, self-calibration, and localization algorithms are those factors that affect system performance. An MScMS-II like optical-based system which involves three generic CCD cameras is developed, aimed at improving the system performance by employing sensors with higher resolution (native resolution is 1360 x1024) and a synchronizer for camera shutter (i.e., time delay of image acquisition by different cameras can be eliminated). This chapter presents details on hardware/software implementation of a prototype system (i.e. the 3-cameras system) and compares the system performance with that of MScMS-II.

5.1 Hardware implementation

The developed prototype involves ordinary CCD cameras as spatially distributed sensors, generic personal computer as data processing unit, and a probe attached with light emitting (new probe) and/or reflective (current probe) target to touch the point of interest in the metrology area. The adopted CCD cameras, of model No: KP-FD140GV (see Fig. 5-1), are manufactured by Hitachi Kokusai Electric Inc. The specifications are listed as follows, see table 5-1:

Table 5-1 Selected specifications of KP-FD140GV camera, for full specs, see Reference (Hitachi Electric).

Imaging device	½- inch progressive scan interline CCD (with on chip micro lens)
Resolution	1360 (H) x1024 (V), ≈1.45M pixels
Pixel Size	4.65 μm
Frame rate	30 frames per second
External dimensions	44 (W) x 29 (H) x 72 (D) mm (not including lens and protrusions)
Mass	Approx. 140g (without lens)

Fig. 5-1 KP-FD140GV CCD camera, manufactured by Hitachi Kokusai Electric Inc.

Besides cameras, some auxiliary components are listed below (see Fig. 5-2), as well as the connection scheme that enables the camera work properly (see Fig. 5-3). The auxiliary components are:

(i) 12 V output AC/DC adapter, to supply power to cameras;
(ii) 24 V output AC/DC adapter, to supply power to LED array;
(iii) hardware trigger, which acts as a synchronizer of all cameras connected in the network;
(iv) circular LED array, emitting high-brightness light to illuminate the retro-reflective targets. The brightness of LED array can be adjustable, according to the working area defined.

A generic system configuration is shown in Fig. 5-4, the prototype has been developed in Quality and Metrology Laboratory of DIGEP (Department of Management and Production Engineering) at Politecnico di Torino. The distributed network consists of 3 optical cameras equipped with circular LED arrays to light the measuring volume. Each camera is able to establish a visual link with specific optical markers (i.e. 40 mm diameter reflective spheres) visible in its "field of view" (FOV). Cameras are equipped by a 1/2-inch 1450000 pixels square lattice progressive scan CCD, and are characterized by an effective resolution of 1360x1024 pixels, a maximum sample rate of 30 Hz, and a shutter variable from 10 to 1/100000 seconds. Image capture may be controlled at desired time using an external trigger signal. The overall sensor set (camera and circular LED array) is 112x112x29 mm in size and weighs about 330 g. Each camera is connected to a DPU via Ethernet cable to transmit images for data processing and real-time tracking. Furthermore, all the cameras are synchronized by a centralised trigger controlled by the same DPU. Auxiliary components to the sensor set are a specific power adapter and a router for the control of data exchange (shown in Fig. 5-3).

Fig. 5-2 Auxiliary components of sensors.

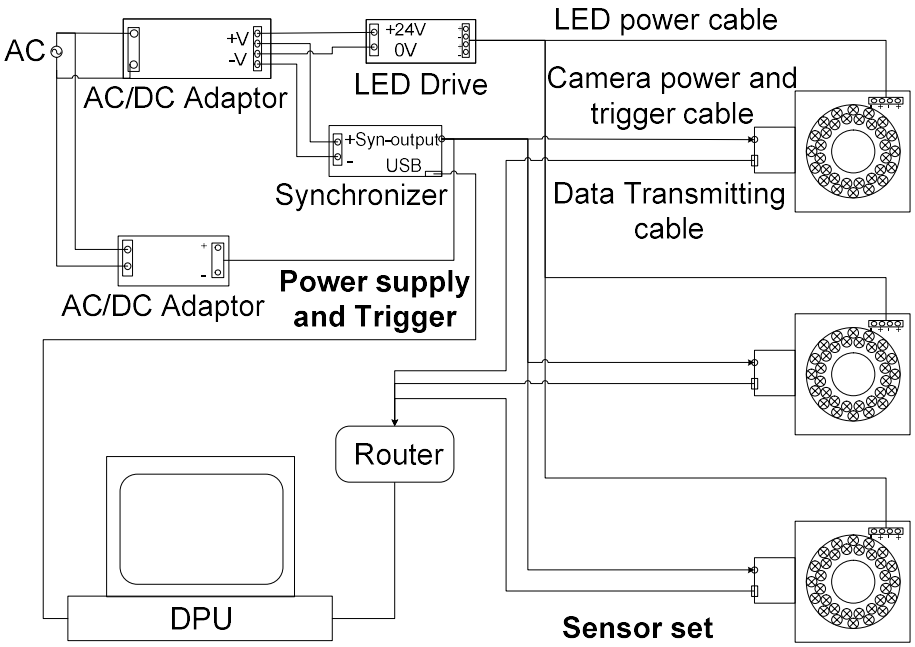

Fig. 5-3 Connection scheme of camera system (an example of 3-cameras network).

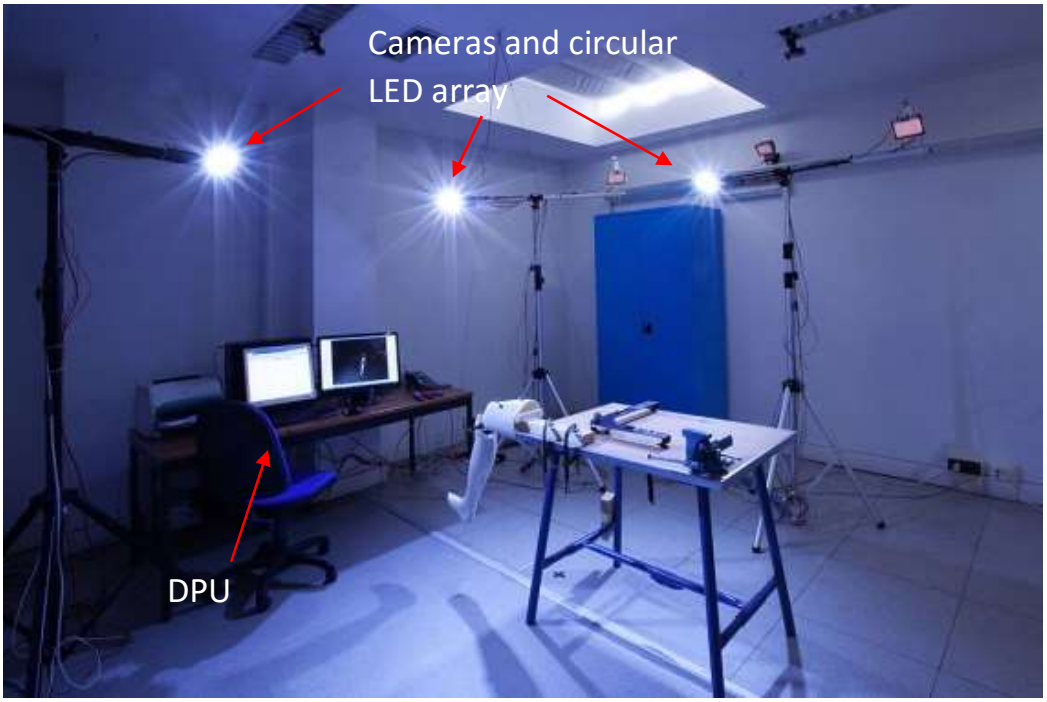

Fig. 5-4 A generic configuration of 3-cameras prototype system (sensors equipped with circular LED array) in a laboratory of DIGEP, Politecnico di Torino (Example of application in the field of human deambulation).

Although there are differences in hardware characteristics and organization, the 3-cameras prototype system shares the same working principles and calibration methods with MScMS-II system, but due to the difference in sensor's sensibility (i.e., IR sensor can extract pixel coordinates of targets by MOT engine, while KP-FD140GV camera needs to extract pixel coordinates by software), there is difference in calibration strategies that can be applied to both systems. Before introducing the calibration strategies, a compressive metrology model of sensors need to be presented first.

5.2 Software (GUI) design

Software associated to the prototype system has been designed to lead the operator to carry out (i) setup, (ii) system calibration and (iii) measurement procedures step by step. It is noteworthy that, the generic CCD sensor involved in the prototype does not have hardware (e.g. MOT in IR sensors) capability to implement image pre-processing, i.e., the image acquired by CCD sensor must be processed by software to extract pixel coordinates of target in image plane.

The setup GUI is shown in Fig. 5-5. In the setup phase, the field of sensing of each sensor is shown to the operator, in order to guide the operator to setup the coverage of FOV and current measuring volume (e.g. the region bounded by red dot-line is defined as the measuring volume, see Fig. 5-5). Furthermore, some technical parameters must be setup in this phase, such as shutter speed, threshold for noise filtering, etc. Afterwards, data collection for system calibration and that for alignment and scaling to a user-defined reference system will be carried out.

System calibration GUI is shown in Fig. 5-6. The aim of this window is to assist the operator to setup those relevant parameters for carrying out system calibration, some of the parameters are explained here:

- INL_TOL: Initial tolerance value for epipolar geometry verification. It influences both the pair-wise point validation through the epipolar geometry computation and the iterative refinement at the end. It should correspond to the expected radial distortion in the cameras. This value is iteratively decreased during the optimization process.
- DO_BA: Do the Bundle Adjustment of the projective reconstruction at the end of the all iterations. It is quite slow for many points and cameras. It may improve the overall accuracy. Often not need at all.
- Nonlinear: Default initial settings for the estimation of the nonlinear distortion
  (1) ... camera view angle?
  (2) ... estimate principal point?
  (3:4) ... estimate parameters of the radial distortion?
  (5:6) ... estimate parameters of the tangential distortion?
- NL_UPDATE: Which nonlinear parameters would you like to update during the global optimization. If you have noisy data with many outliers you may want to stabilize the

optimization by fixing some parameters. It also depends on what parameters are you actually using for undoing distortions.

- DO_GLOBAL_ITER: Option to perform global optimization.
- GLOBAL_ITER_MAX: Maximum number of iterations for the global optimization.
- GLOBAL_ITER_THR: Stopping condition for the global optimization. The process ends if the maximum of the reprojection error (average in each of the cameras) is lower than this threshold.
- UNDO_RADIAL: Option to correct lens distortion using the parameters estimated.

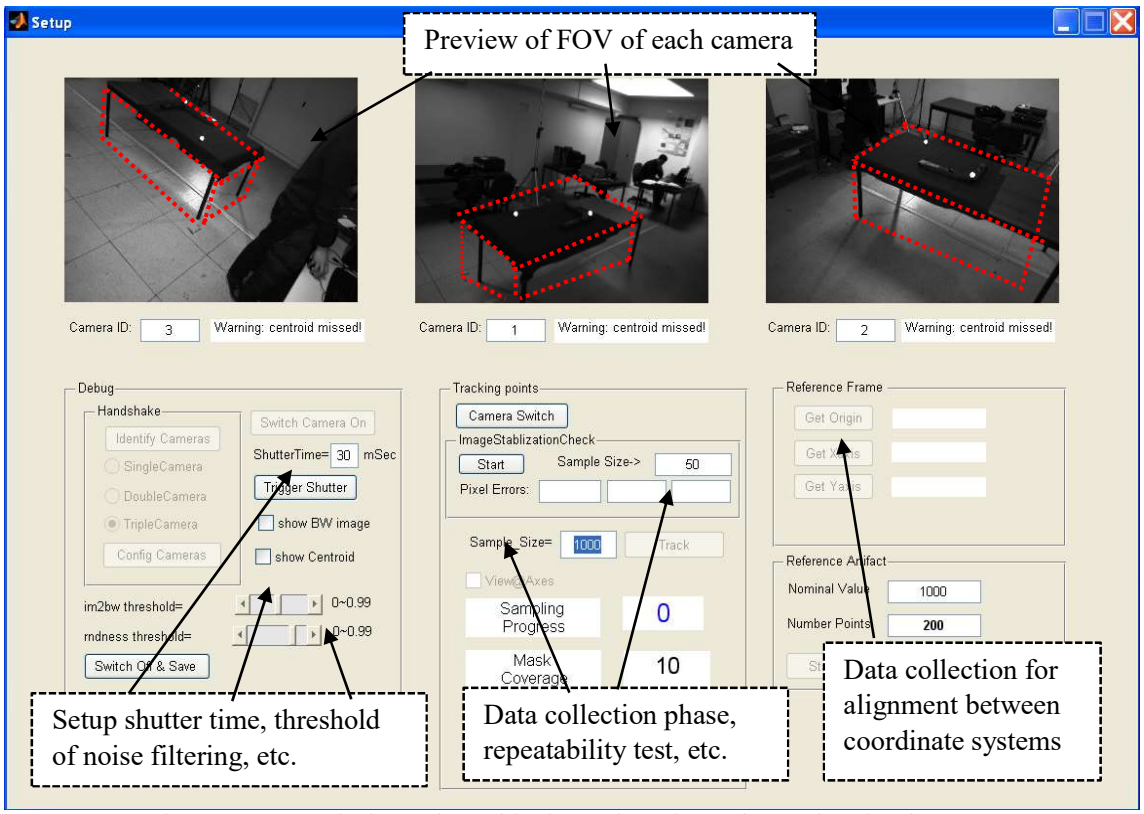

Fig. 5-5 Setup window of graphical user interface of associated software.

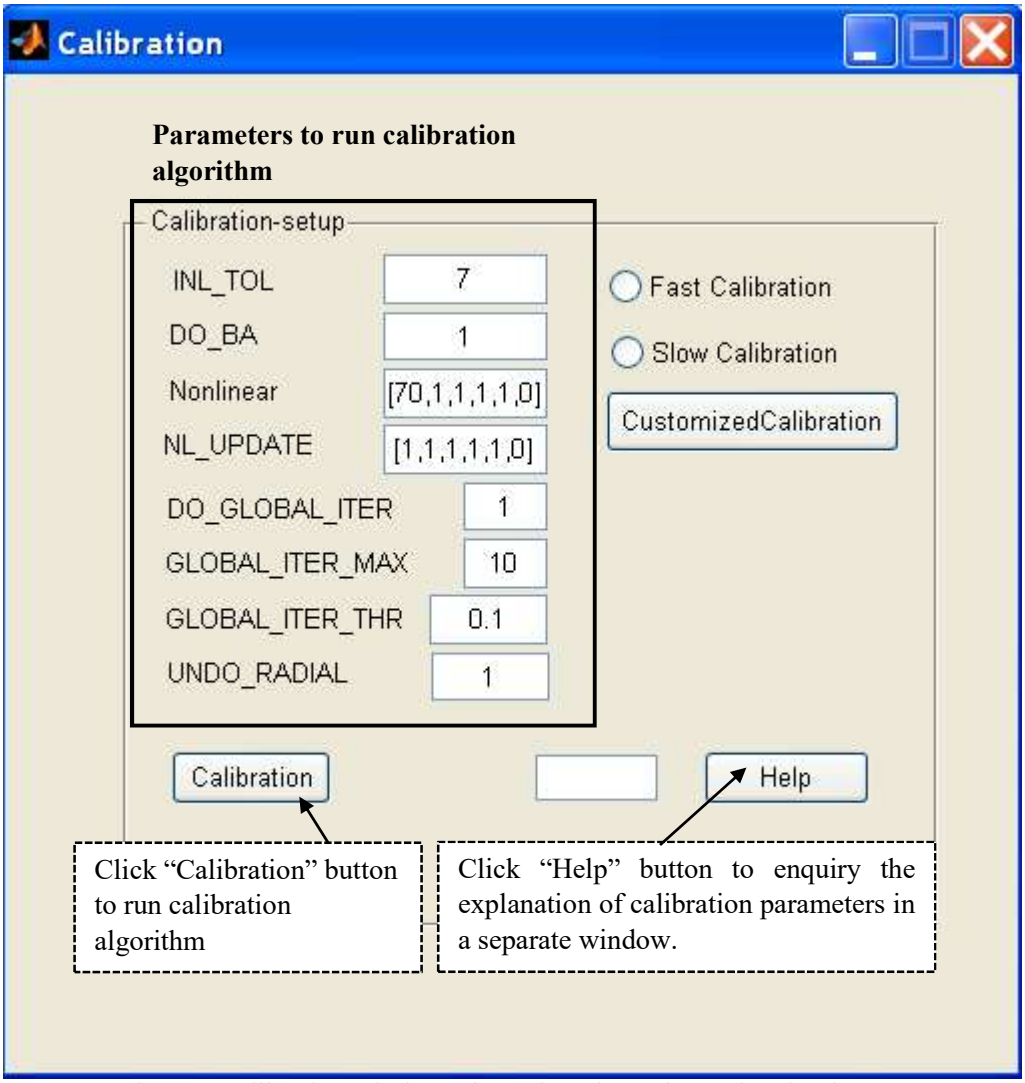

Fig. 5-6 Calibration window of user interface of associated software.

Once system calibration has been done, the internal and external parameters have been estimated properly, it comes to the measurement phase, the GUI for doing measurement (e.g., point inspection, length inspection, geometric features inspections, etc.) is shown in Fig. 5-7. Figure 5-7 shows the dimensional inspection of a cylinder, the software outputs the estimated radius, center of radius, as well as the axis vector of the cylinder. Besides the parameters estimated, the recorded points and best-fitted geometrical features can be plotted in the GUI as well.

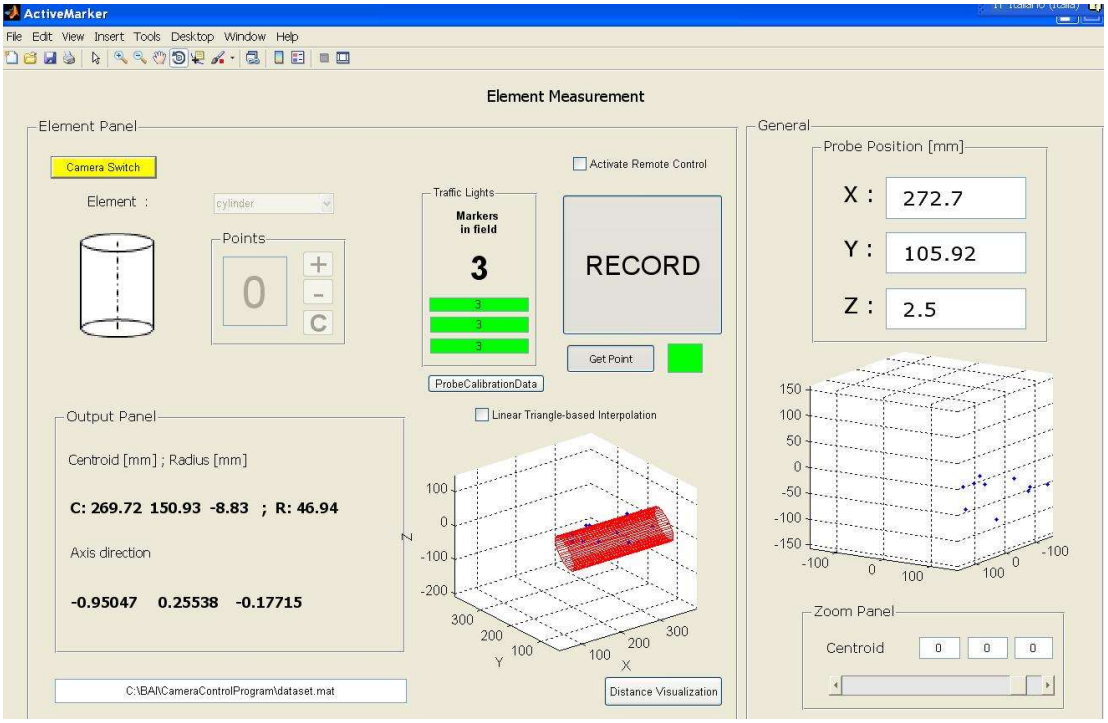

Fig. 5-7 Dimensional inspection window (e.g. a cylinder inspection task is selected).

5.3 Summary of 3-cameras prototype system

A preliminary test has been carried out in order to investigate (i) the system stability and (ii) the metrological performance in length inspection of the prototype system. An artifact (see Fig. 3-7) is involved, with calibrated length shown in table 3-1. The reported uncertainties by means of CMM in table 3-1 are lower than 3 μm, which is adequate for the expected performance of the system (around 0.1 mm). It is hereby stated that, only the leftmost and rightmost spheres with calibrated distance 1001.030 mm are involved in the length inspection. Specifically, the test configuration is summarized as follows:

- a set of 3 cameras (model: KP-FD140GV) is arranged in triangular layout in the working environment (see Fig. 5-4);
- the measurement volume is about $4.0\times1.5\times2.0$ m^3;
- a calibrated artifact with nominal length 1001.030 mm (table 3-1) is involved;
- a sampling frequency of 30 Hz is used for data acquisition.

1) System stability has been evaluated on s=15 different positions, located at a grid-based layout within the measurement volume (shown in Fig. 5-8). For each position, 0-ball of the artifact has been kept in a stationary condition, replicating the measurement k=100

times. Results are reported in table 5-2, in terms of sample mean and standard deviation of the reconstructed coordinates of 0-ball.

2) System performance in length inspection has been tested on s=5 different positions, linearly distributed within the measurement volume. The test has been carried out by repeating the measurement k=100 times for each position, repositioning the artifact in the same position for each measurement. Results of repeatability tests are reported in table 5-3, in terms of sample mean and standard deviation of the measured length of the artifact. Fig. 5-9 shows the distribution of measured length against the z-coordinates of the position.

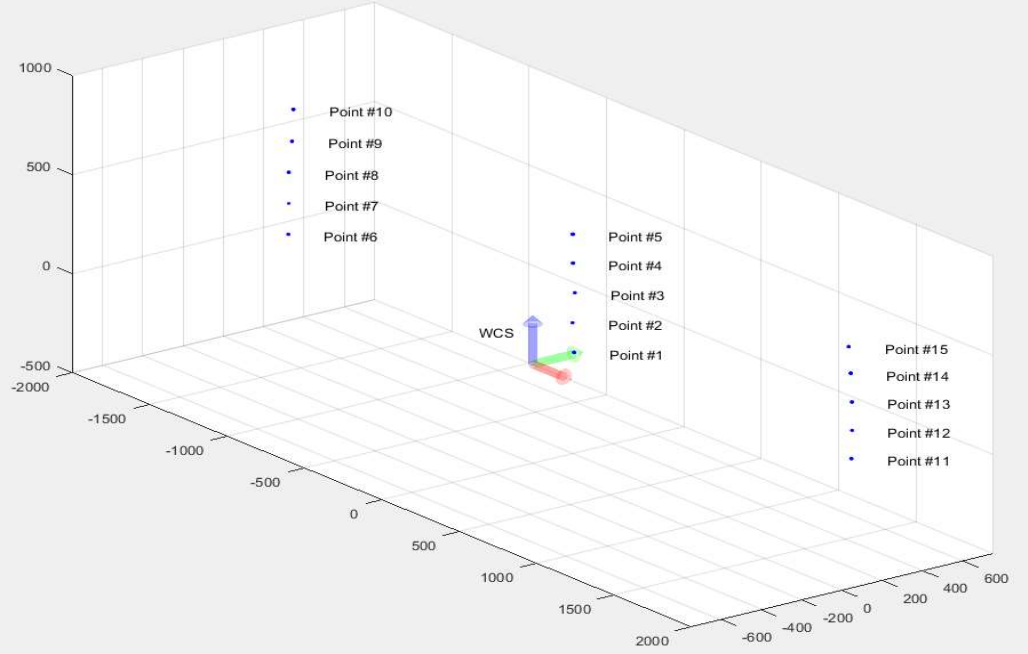

Fig. 5-8 Grid-based layout of measured points in stability test.

Table 5-2 Mean and standard deviation results for stability test. Sample mean coordinates refer to a user-defined room-aligned reference coordinate system. (unit: mm)

Position	$\overline{x}$	$\overline{y}$	$\overline{z}$	$\hat{\sigma}_x$	$\hat{\sigma}_y$	$\hat{\sigma}_z$
#1	21.41	188.50	19.19	0.17	0.15	0.06
#2	18.96	182.49	169.86	0.16	0.05	0.06
#3	23.09	191.02	320.09	0.13	0.08	0.06
#4	20.26	184.05	470.55	0.17	0.10	0.03
#5	27.83	176.96	620.34	0.19	0.12	0.05
#6	-1814.14	179.84	28.90	0.09	0.02	0.05
#7	-1809.60	178.42	186.57	0.05	0.03	0.05
#8	-1807.86	177.24	344.06	0.26	0.19	0.05
#9	-1799.33	186.70	501.12	0.13	0.06	0.03
#10	-1805.31	197.96	657.40	0.17	0.15	0.04
#11	1738.67	246.15	20.03	0.18	0.07	0.05
#12	1741.30	247.50	162.62	0.13	0.06	0.07
#13	1739.21	248.51	305.16	0.23	0.03	0.05
#14	1730.11	249.69	447.04	0.32	0.04	0.08
#15	1738.90	232.74	588.08	0.17	0.03	0.04

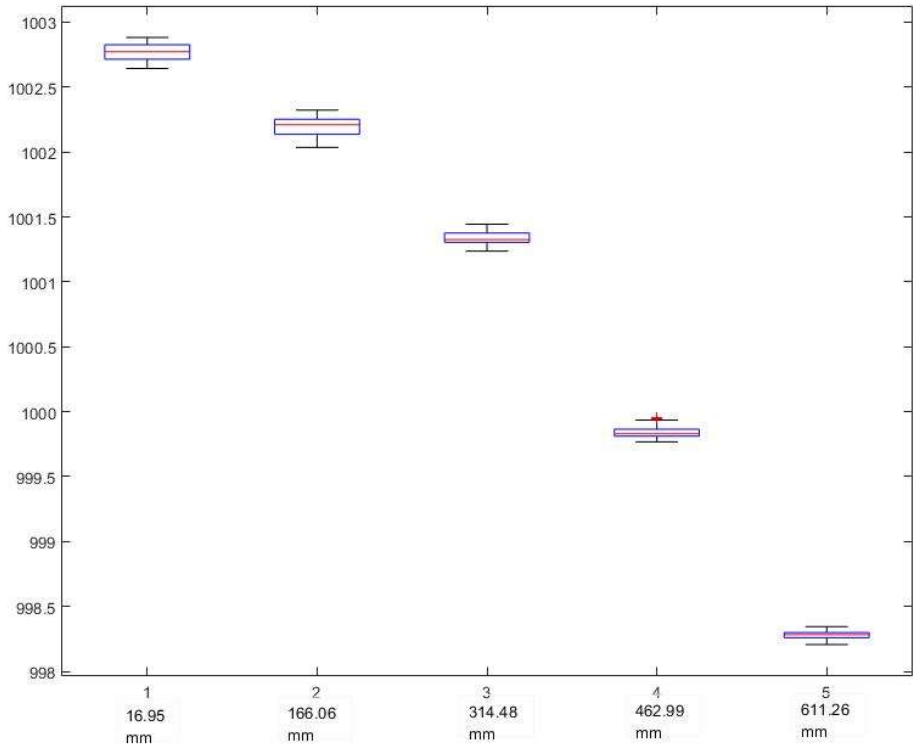

Fig. 5-9 Measured length of artifact against z-coordinate of the location of artifact.

Table 5-3 Repeatability test of length inspection. (unit: mm)

Position	$\overline{L}$	$\hat{\sigma}_L$	$\overline{x}$	$\overline{y}$	$\overline{z}$
#1	1002.76	0.06	10.48	162.65	16.95
#2	1002.19	0.07	-1.04	169.28	166.06
#3	1001.33	0.04	-13.08	167.30	314.48
#4	999.84	0.04	-4.55	173.73	462.99
#5	998.27	0.03	7.84	166.10	611.26

According to the results obtained by these experimental tests, the prototype system slightly outperforms the MScMS-II system in terms of system stability (see section 2.2.7, refer to table 2-1). It may be partially due to use of high resolution sensors (i.e., 1360x1024 (KP-FD140GV Camera) vs. 128x96 (IR sensor)), but other factors (e.g., number of sensors, sensors positioning, calibration result, localization algorithm, etc.) may influence the results as well.

In terms of performance in length measurement, the result shows some relation (linear or quadratic type, by initial speculation) between the mean value of length measured and the z-coordinate of the position where the bar has been placed. The reason that explains the observations could be lens distortion effect. Generic optical-based sensors are mounted with focal lens in order to get focused images, therefore, lens distortion cannot be totally ignored, especially in metrology applications. As a matter of fact, lens distortion has stronger effect when measured point is farther from the principal point (i.e. the center of image plane) in the image plane. Moreover, according to the system configuration, sensors have been positioned close to the ceiling in the room and oriented downwards to cover the measuring volume, thus changes of z-coordinate result in changes of distance between the measured 2D point and principal point in the image plane. Therefore, when measured 2D points are approaching the border of the image plane, distorted 2D points will result in a distorted reconstruction of 3D points.

In order to inspect in details the relation, further experimental tests have to be carried out and corrective algorithm needs to be developed.

In summary, the developed prototype system is a MScMS-II like, distributed system based on generic CCD cameras, due to its involvement of general use hardware, it is easy to maintain and subject to multiple use. Although it shares similar working principles with MScMS-II system, some native characteristics distinguish it from MScMS-II system.

(i) adjustable aperture and focal length of lens mounted on the sensor, adaptable to complex indoor and outdoor lighting conditions;

(ii) only visual link between sensors and target established, theoretically unlimited number of targets (comparing to the fact that at most 4 targets are trackable in MScMS-II case), no additional cost for each target;
(iii) comprehensive sensing model, applicable to multiple calibration tools, e.g. calibration toolbox in MATLAB software (J.Y Bouguet 2015), single target self-calibration algorithm (T. Svoboda et al. 2005), etc.;
(iv) synchronized shutter trigger and high speed data transferring channel, result in least uncertainty due to time delay in data acquisition and transferring.

The main differences in hardware configuration between two systems are listed in table 5-4:

Table 5-4 Comparison between MScMS-II system and CCD camera prototype system

	MScMS-II	**CCD camera prototype system**
sensor type	IR sensor with MOT engine (at most 4 targets simultaneously trackable)	Generic CCD sensor, no MOT engine (target detection by software, unlimited number of targets trackable)
native resolution	128×96	1360×1024
FOV	45°×30° (approx.)	60°×45° (approx.)
sampling rate	100 Hz	30 Hz
data transfer media	Bluetooth	GigE internet cable
number of sensors	6 sensors involved in current system	3 sensors involved in current prototype
synchronizer	no	yes

6. Conclusions

This dissertation studies and characterizes an optical-based multi-camera system for indoor dimensional measurements (MScMS-II). The design and prototype development of a new concept probe involved in the system, named as "smart probe", has been proposed, as a possible evolution and improvement to the MScMS-II system.

Factors that influence system performance have been discussed and some error correction models for performance improvement have been presented as well. Furthermore, a diagnostic technique for monitoring system parameters is proposed, as an integrated part of the calibration software associated with the system, no additional operation is required. This is a future direction of software design of the metrology system, i.e., least effort from the operator will be needed.

This chapter summarizes the main contributions of the research work and the related challenges. The main contributions of this thesis are outlined hereafter.

Design and implementation of a new concept probe involved in MScMS-II system

A novel IR optical-based system—the MScMS-II—has been proposed in recent years, which is designed as an affordable solution to perform low-cost indoor coordinate measurements of large-sized objects. A contact probe (current probe) is involved in MScMS-II, which consists of (i) a slim rod which is easy to be held by human and robot arm, (ii) two retro-reflective spherical markers that can be detectable by IR sensors, whenever they are illuminated by IR light in the sensing filed of sensors, and (iii) a stainless steel stick with ultra-hard ruby ball-tip that is used to touch the object to be measured. The coordinates of ball-tip can be determined by localizing the two markers in 3D space and knowing the geometry of the probe (i.e., the distance between two markers and that between the tip and marker). The current probe meets all the requirements of localization with such a simple design. While it has drawbacks such as (i) the need of external illuminator and (ii) the lack of monitoring capability for environmental conditions.

The concept of new probe emerges with the need for an improvement to current probe, in at least the outlined aspects:

(i) it performs better in a highly reflective environment, and it reduces the influence on the environment to a minimum level, by removing the illuminator around the sensor;

(ii) it performs better in a noisy working conditions (i.e., with changing temperature and humidity, kinematic variations, etc.) that are substantially relevant to the measure result of an optical-based system;

(iii) it performs better in localization of probe tip, due to the redundancy resulted from more makers equipped;

(iv) it performs better in collaboration with the operator, by integrating antenna for wireless communication and data transfer to DPU.

A national patent (Fiorenzo Franceschini et al. 2016) has been issued of the design of new probe based on the novelty listed above, and a prototype has been implemented with active markers (i.e. markers illuminated by internal light source) and the prototype has been verified to work properly with current system.

Implementation of a diagnostic tool for monitoring the calibration results

The correctness of estimation of calibration results are of great relevance to the metrological performance of optical-based multi-camera systems. While, instead of using hardware effort or calibrated artifacts (which are proved to be costly and time-consuming), a diagnostic tool based on multivariate control charts has been proposed in the thesis and it turns the calibration data into the diagnosis directly, with no additional operation. The proposed method separate the system parameters into internal parameters and external ones, and design a proper control chart to monitor the stability of internal parameters, since the external ones are ever-changing with the specific system layout. Furthermore, based on the proposed method, two well-known calibration approaches are compared and analyzed, and a hybrid calibration approach could be scheduled for the MScMS-II system.

Implementation of an MScMS-II like, custom-made prototype system based on 3 generic CCD cameras

the developed prototype system is a MScMS-II like, distributed system based on generic CCD cameras, due to its involvement of general use hardware, it is easy to maintain and subject to multiple use. Although it shares similar working principles with MScMS-II system, some native characteristics distinguish it from MScMS-II system:

(i) adjustable aperture and focal length of lens mounted on the sensor, adaptable to complex indoor and outdoor lighting conditions;
(ii) only visual link between sensors and target established, theoretically unlimited number of targets (comparing to the fact that at most 4 targets are trackable in MScMS-II case), no additional cost for each target;
(iii) comprehensive sensing model, applicable to multiple calibration tools, e.g. calibration toolbox in MATLAB software (J.Y Bouguet 2015), single target self-calibration algorithm (T. Svoboda et al. 2005), etc.;
(iv) synchronized shutter trigger and high speed data transferring channel, result in least uncertainty due to time delay in data acquisition and transferring.

References:

B Aebischer and B Braunecker (2003). Total station for measuring the 3-D position and orientation of a rigid body. Proceedings of 6th Conference on Optical.

Aicon. "http://aicon3d.com/start.html." Retrieved 31 Dec, 2015.

Hideki Aoyama, M Kawai, T Kishinami and N Taniguchi (1989). "A new method for detecting the contact point between a touch probe and a surface." CIRP Annals-Manufacturing Technology **38**(1): 517-520.

Ou Bai, Fiorenzo Franceschini, Maurizio Galetto, Luca Mastrogiacomo and Domenico A Maisano (2014). A Comparison of Two Different Approaches to Camera Calibration in LSDM Photogrammetric Systems. ASME 2014 12th Biennial Conference on Engineering Systems Design and Analysis. Copenhagen, American Society of Mechanical Engineers.

IEC BIPM, ILAC IFCC, IUPAC ISO and OIML IUPAP (2008). The international vocabulary of metrology—basic and general concepts and associated terms (VIM), JCGM 200: 2008.

Ake Björck (1996). Numerical methods for least squares problems, Siam.

J.Y Bouguet (2015). "Camera Calibration Toolbox for Matlab." Retrieved 31 Dec, 2015, from http://www.vision.caltech.edu/bouguetj/calib_doc/index.html.

A. W. Burner, R. H. Radeztsky and T. Liu (1997). Videometric applications in wind tunnels. Proceedings of SPIE - The International Society for Optical Engineering.

Simone Carmignato (2009). Experimental study on performance verification tests for coordinate measuring systems with optical distance sensors. IS&T/SPIE Electronic Imaging, International Society for Optics and Photonics.

F. Chen, G. M. Brown and M. Song (2000). "Overview of three-dimensional shape measurement using optical methods." Optical Engineering **39**(1): 10-22.

Paul Debrule, Ed Saade and Andrew Palmer (1995). Laser line scan. Man-Made Objects on the Seafloor Discovery, Investigation and Recovery 1995, Society of Underwater Technology.

Kutluyil Doğançay (2005). "Bearings-only target localization using total least squares." Signal Processing **85**(9): 1695-1710.

F. Du, Z. Chen and X. Tang (2012). "Precision analysis of iGPS measurement field and its application." Hangkong Xuebao/Acta Aeronautica et Astronautica Sinica **33**(9): 1737-1745.

C BROWN Duane (1971). "Close-range camera calibration." Photogrammetric engineering **37**(8): 855-866.

Hitachi Electric. "http://www.hitachi-kokusai.co.jp/global/products/video/camera/fa_camera/gige_vision/kp-fd140gv.html." Retrieved 31 Dec, 2015.

Chris J Evans, Robert J Hocken and W Tyler Estler (1996). "Self-calibration: reversal, redundancy, error separation, and 'absolute testing'." CIRP Annals-Manufacturing Technology **45**(2): 617-634.

FARO. "http://www.faro.com/en-us/home." Retrieved 31 Dec, 2015.

Fiorenzo Franceschini, Maurizio Galetto, Domenico Augusto Maisano, Luca Mastrogiacomo and Ou Bai (2016). Dispositivo Tastatore, Marker Per Dispositivo Tastatore E Sistema Di Misura Per Effettuare Misure Fotogrammetriche Di Oggetti Di Grandi Dimensioni. L'Ufficio Italiano Brevetti e Marchi. Italy. **102016000001556**.

Martin A Fischler and Robert C Bolles (1981). "Random sample consensus: a paradigm for model fitting with applications to image analysis and automated cartography." Communications of the ACM **24**(6): 381-395.

Marek Franaszek, Geraldine S Cheok and Kamel S Saidi (2011). "Gauging the repeatability of 3-d imaging systems by sphere fitting." Instrumentation and Measurement, IEEE Transactions on **60**(2): 567-576.

F. Franceschini, M. Galetto, D. Maisano and L. Mastrogiacomo (2014). "Large-scale dimensional metrology (LSDM): From tapes and theodolites to multi-sensor systems." International Journal of Precision Engineering and Manufacturing **15**(8): 1739-1758.

F. Franceschini, D. Maisano and L. Mastrogiacomo (2009). "Mobile spatial coordinate measuring system (MScMS) and CMMs: A structured comparison." International Journal of Advanced Manufacturing Technology **42**(11-12): 1089-1102.

Fiorenzo Franceschini, Maurizio Galetto, Domenico Maisano and Luca Mastrogiacomo (2009). "On-line diagnostics in the mobile spatial coordinate measuring system (MScMS)." Precision Engineering **33**(4): 408-417.

Fiorenzo Franceschini, Maurizio Galetto, Domenico Maisano, Luca Mastrogiacomo and Barbara Pralio (2011). Distributed large-scale dimensional metrology: new insights. London, UK, Springer Science & Business Media.

J. Fryer, H. Mitchell and J.H. Chandler (2007). Applications of 3D measurement from images, Whittles.

M. Galetto, Pralio B (2010). "Optimal sensor positioning for large scale metrology applications." Precision Engineering **34**(3): 563-577.

M. Galetto, L. Mastrogiacomo and B. Pralio (2010a). "The Mobile Spatial coordinate Measuring System II (MScMS-II): System description and preliminary assessment of the measurement uncertainty." International Journal of Metrology and Quality Engineering **1**(2): 111-119.

M. Galetto, L. Mastrogiacomo and B. Pralio (2010b). "A wireless sensor network-based approach to large-scale dimensional metrology." International Journal of Computer Integrated Manufacturing **23**(12): 1082-1094.

M. Galetto, L. Mastrogiacomo, B. Pralio and C. Spagnolo (2010c). Indoor environmental mapping by means of autonomous guided agents. ASME 2010 10th Biennial Conference on Engineering Systems Design and Analysis, ESDA2010.

Maurizio Galetto and Luca Mastrogiacomo (2013). "Corrective algorithms for measurement improvement in MScMS-II (mobile spatial coordinate measurement system)." Precision Engineering **37**(1): 228-234.

Maurizio Galetto, Luca Mastrogiacomo, Giovanni Moroni and Stefano Petrò (2013). "Volumetric error compensation for the MScMS-II." Procedia CIRP **10**: 98-104.

Maurizio Galetto, Luca Mastrogiacomo, Giovanni Moroni and Stefano Petrò (2015). "Artifact-based Calibration and Performance Verification of the MScMS-II." Procedia CIRP **27**: 77-83.

Maurizio Galetto, Luca Mastrogiacomo and Barbara Pralio (2010a). "MScMS-II: an innovative IR-based indoor coordinate measuring system for large-scale metrology applications." The International Journal of Advanced Manufacturing Technology **52**(1): 291-302.

Maurizio Galetto, Luca Mastrogiacomo, Barbara Pralio and Cristina Spagnolo (2010b). Indoor environmental mapping by means of autonomous guided agents. ASME 2010 10th Biennial Conference on Engineering Systems Design and Analysis, American Society of Mechanical Engineers.

Gene H Golub and Christian Reinsch (1970). "Singular value decomposition and least squares solutions." Numerische mathematik **14**(5): 403-420.

H. González-Jorge, B. Riveiro, P. Arias and J. Armesto (2012). "Photogrammetry and laser scanner technology applied to length measurements in car testing laboratories." Measurement: Journal of the International Measurement Confederation **45**(3): 354-363.

John C Gower and Garmt B Dijksterhuis (2004). Procrustes problems. Oxford, UK, Oxford University Press Oxford.

Richard I Hartley and Peter Sturm (1997). "Triangulation." Computer vision and image understanding **68**(2): 146-157.

Richard Hartley and Andrew Zisserman (2004). Multiple View Geometry in Computer Vision, Cambridge University Press.

Hexagon. "http://www.hexagon.com/en/index.htm." Retrieved 31 Dec, 2015.

Bernhard Hofmann-Wellenhof, Herbert Lichtenegger and James Collins (2012). Global positioning system: theory and practice, Springer Science & Business Media.

Theodore H Hopp and Mark S Levenson (1995). "Performance measures for geometric fitting in the NIST algorithm testing and evaluation program for coordinate measurement systems." JOURNAL OF RESEARCH-NATIONAL INSTITUTE OF STANDARDS AND TECHNOLOGY **100**: 563-574.

Harold Hotelling (1947). "Multivariate quality control." Techniques of statistical analysis.

EB Hughes, A Wilson and GN Peggs (2000). "Design of a high-accuracy CMM based on multi-lateration techniques." CIRP Annals-Manufacturing Technology **49**(1): 391-394.

ISO (2009). ISO 10360-2: Geometrical product specifications (GPS) – Acceptance and reverification tests for coordinate measuring machines (CMM) –Part 2: CMMs used for measuring linear dimensions, International Standard Organization.

J. Jamshidi, A. Kayani, P. Iravani, P. G. Maropoulos and M. D. Summers (2010). "Manufacturing and assembly automation by integrated metrology systems for aircraft wing fabrication." Proceedings of the Institution of Mechanical Engineers, Part B: Journal of Engineering Manufacture **224**(1): 25-36.

J Jeong and K Kim (1999). "Generation of tool paths for machining free-form pockets with islands using distance maps." The International Journal of Advanced Manufacturing Technology **15**(5): 311-316.

Rudolph Emil Kalman (1960). "A new approach to linear filtering and prediction problems." Journal of basic Engineering **82**(1): 35-45.

Jean-Pierre Kruth, Paul Vanherck and Lieven De Jonge (1994). "Self-calibration method and software error correction for three-dimensional coordinate measuring machines using artefact measurements." Measurement **14**(2): 157-167.

Kam C Lau and Robert J Hocken (1987). Three and five axis laser tracking systems, Google Patents.

Charles L Lawson and Richard J Hanson (1974). Solving least squares problems, SIAM.

Shuh-Ren Liang and Alan C Lin (2002). "Probe-radius compensation for 3D data points in reverse engineering." Computers in Industry **48**(3): 241-251.

YC Lin and WI Sun (2003). "Probe radius compensated by the multi-cross product method in freeform surface measurement with touch trigger probe CMM." The International Journal of Advanced Manufacturing Technology **21**(10-11): 902-909.

HC Longuet-Higgins (1981). "A computer algorithm for reconstructing a scene from two projections." Nature **293**: 133-135.

Cynthia A Lowry and Douglas C Montgomery (1995). "A review of multivariate control charts." IIE transactions **27**(6): 800-810.

Thomas Luhmann, Stuart Robson, Stephen Kyle and Ian Harley (2006). Close range photogrammetry: Principles, methods and applications. Dunbeath,UK, Whittles.

D. A. Maisano, J. Jamshidi, F. Franceschini, P. G. Maropoulos, L. Mastrogiacomo, A. R. Mileham and G. W. Owen (2009). "A comparison of two distributed large-volume measurement systems: The mobile spatial co-ordinate measuring system and the indoor global positioning system." Proceedings of the Institution of Mechanical Engineers, Part B: Journal of Engineering Manufacture **223**(5): 511-521.

Mapvision. "http://www.mapvision.fi/en/." Retrieved 31 Dec, 2015.

P. G. Maropoulos, Y. Guo, J. Jamshidi and B. Cai (2008). "Large volume metrology process models: A framework for integrating measurement with assembly planning." CIRP Annals - Manufacturing Technology **57**(1): 477-480.

Donald W Marquardt (1963). "An algorithm for least-squares estimation of nonlinear parameters." Journal of the society for Industrial and Applied Mathematics **11**(2): 431-441.

JRR Mayer, YA Mir, F Trochu, A Vafaeesefat and M Balazinski (1997). "Touch probe radius compensation for coordinate measurement using kriging interpolation." Proceedings of the Institution of Mechanical Engineers, Part B: Journal of Engineering Manufacture **211**(1): 11-18.

Edward M Mikhail, James S Bethel and J Chris McGlone (2001). Introduction to modern photogrammetry. New York, USA, John Wiley & Sons Inc.

Konica Minolta. "http://www.konicaminolta.com/." Retrieved 31 Dec, 2015.

J. Mitchell, A. Spence, M. Hoang and A. Free (2004). Sensor fusion of laser trackers for use in large-scale precision metrology. Proceedings of SPIE - The International Society for Optical Engineering.

Douglas C Montgomery (2007). Introduction to statistical quality control. Hoboken, New Jersey, John Wiley & Sons.

J. E. Muelaner, Z. Wang, O. Martin, J. Jamshidi and P. G. Maropoulos (2010). "Estimation of uncertainty in three-dimensional coordinate measurement by comparison with calibrated points." Measurement Science and Technology **21**(2).

Jody E Muelaner, Z Wang, Jafar Jamshidi, Paul Maropoulos, Antony R Mileham, EB Hughes and AB Forbes (2008). iGPS-An initial assessment of technical and deployment capability. 3rd International Conference on Manufacturing Engineering, University of Bath.

A. Nüchter, H. Surmann, K. Lingemann and J. Hertzberg (2003). Consistent 3D model construction with autonomous mobile robots. Lecture Notes in Artificial Intelligence (Subseries of Lecture Notes in Computer Science).

A. R. Norman, A. Schönberg, I. A. Gorlach and R. Schmitt (2013). "Validation of iGPS as an external measurement system for cooperative robot positioning." International Journal of Advanced Manufacturing Technology **64**(1-4): 427-446.

Nikon Metrology NV. "http://www.nikonmetrology.com/en_EU/." Retrieved 31 Dec, 2015.

Jae-jun Park, Kihwan Kwon and Nahmgyoo Cho (2006). "Development of a coordinate measuring machine (CMM) touch probe using a multi-axis force sensor." Measurement Science and Technology **17**(9): 2380.

G. N. Peggs, P. G. Maropoulos, E. B. Hughes, A. B. Forbes, S. Robson, M. Ziebart and B. Muralikrishnan (2009). "Recent developments in large-scale dimensional metrology." Proceedings of the Institution of Mechanical Engineers, Part B: Journal of Engineering Manufacture **223**(6): 571-595.

API Automated Precision. "http://www.apisensor.com/." Retrieved 31 Dec, 2015.

M. J. Puttock (1978). "LARGE - SCALE METROLOGY." Gen Assem of CIRP, 28th, Manuf Technol **27**(1): 351-356.

M. Ribo and M. Brandner (2005). State of the art on vision-based structured light systems for 3D measurements. Proceedings of the 2005 IEEE International Workshop on Robotic Sensors: Robotic and Sensor Environments, ROSE 2005.

Joaquim Salvi, Jordi Pages and Joan Batlle (2004). "Pattern codification strategies in structured light systems." Pattern recognition **37**(4): 827-849.

J. Santolaria, J. Conte and M. Ginés (2013). "Laser tracker-based kinematic parameter calibration of industrial robots by improved CPA method and active retroreflector." International Journal of Advanced Manufacturing Technology **66**(9-12): 2087-2106.

E. Savio, L. De Chiffre and R. Schmitt (2007). "Metrology of freeform shaped parts." CIRP Annals - Manufacturing Technology **56**(2): 810-835.

R. Schmitt, S. Nisch, A. Schönberg, F. Demeester and S. Renders (2010). Performance evaluation of iGPS for industrial applications. 2010 International Conference on Indoor Positioning and Indoor Navigation, IPIN 2010 - Conference Proceedings.

FW Scholz and TJ Tosch (1994). "Small sample uni-and multivariate control charts for means." Proc Amer Statistical Assoc, Quality and Productivity Section: 17-22.

Amnon Shashua and Shai Avidan (1996). The rank 4 constraint in multiple (≥ 3) view geometry. Computer Vision—ECCV'96, Springer**:** 196-206.

Tony Slotwinski and Patrick Blanckaert (2007). Frequency modulated coherent laser radar technology. Proceedings of the 3rd workshop on optical measurement techniques, OPTIMES. Optical Measurement Technologies for Structures and Systems.

C-K Song and S-W Kim (1997). "Reverse engineering: autonomous digitization of free-formed surfaces on a CNC coordinate measuring machine." International Journal of Machine Tools and Manufacture **37**(7): 1041-1051.

Joe H Sullivan and William H Woodall (1996). "A comparison of multivariate control charts for individual observations." Journal of Quality Technology **28**(4): 398-408.

T. Svoboda. "http://cmp.felk.cvut.cz/~svoboda/." Retrieved 31 Dec, 2015.

T. Svoboda, D. Martinec and T. Pajdla (2005). "A convenient multicamera self-calibration for virtual environments." Presence: Teleoperators and Virtual Environments **14**(4): 407-422.

Toshiyuki Takatsuji, Mitsuo Goto, Tomizo Kurosawa, Yoshihisa Tanimura and Yoshihiko Koseki (1998). "The first measurement of a three-dimensional coordinate by use of a laser tracking interferometer system based on trilateration." Measurement Science and Technology **9**(1): 38.

Nola D Tracy (1992). "Multivariate control charts for individual observations." Jour. Quality Technology **24**(2): 88-95.

Roger Y Tsai (1987). "A versatile camera calibration technique for high-accuracy 3D machine vision metrology using off-the-shelf TV cameras and lenses." Robotics and Automation, IEEE Journal of **3**(4): 323-344.

Nick Van Gestel, Steven Cuypers, Philip Bleys and Jean-Pierre Kruth (2009). "A performance evaluation test for laser line scanners on CMMs." Optics and Lasers in Engineering **47**(3): 336-342.

Greg Welch and Gary Bishop (2006). An introduction to the kalman filter. Department of Computer Science, University of North Carolina, Chapel Hill, NC, unpublished manuscript.

K Wendt, M Franke and F Härtig (2010). "Mobile multi-lateration measuring system for high accurate and traceable 3D measurements of large objects." Proceedings of the 10th ISMQC Paper(25): 1-4.

Wikipedia. "https://en.wikipedia.org/wiki/Coordinate-measuring_machine#Description." Retrieved 31 Dec, 2015.

Wikipedia. "https://en.wikipedia.org/wiki/Euclidean_distance." Retrieved 31 Dec, 2015.

William H Woodall, Roger W Hoerl, Andrew C Palm and Donald J Wheeler (2000). "Controversies and contradictions in statistical process control/Discussion/Response." Journal of Quality Technology **32**(4): 341.

A Woźniak, JRR Mayer and M Bałaziński (2009). "Stylus tip envelop method: corrected measured point determination in high definition coordinate metrology." The International Journal of Advanced Manufacturing Technology **42**(5-6): 505-514.

Zhenhua Xiong and Zexiang Li (2003). "Probe radius compensation of workpiece localization." Journal of manufacturing science and engineering **125**(1): 100-104.

Song Zhang and Peisen S Huang (2006). "Novel method for structured light system calibration." Optical Engineering **45**(8): 083601-083601-083608.

Zhengyou Zhang (1999). Flexible camera calibration by viewing a plane from unknown orientations. Computer Vision, 1999. The Proceedings of the Seventh IEEE International Conference on, IEEE.

Zhengyou Zhang (2000). "A flexible new technique for camera calibration." Pattern Analysis and Machine Intelligence, IEEE Transactions on **22**(11): 1330-1334.

Yin Zhongwei, Zhang Yuping and Jiang Shouwei (2003). "Methodology of NURBS surface fitting based on off-line software compensation for errors of a CMM." Precision Engineering **27**(3): 299-303.